COUPLING: IMPACT AND IMPLICATIONS FOR HIGH-RESOLUTION TIME-LAPSE SEISMIC SURVEYING

BY

Shelby L. Walters

Submitted to the graduate degree program in Geology
and the Faculty of the Graduate School of the University of Kansas
In partial fulfillment of the requirements for the degree of
Master's of Science

_____
Richard D. Miller, Chairperson

_____
Georgios P. Tsoflias

_____
Jennifer A. Roberts

Date defended: _____

The Thesis Committee for Shelby L. Walters certifies
That this is the approved Version of the following thesis:

COUPLING: IMPACT AND IMPLICATIONS FOR HIGH-RESOLUTION
TIME-LAPSE SEISMIC SURVEYING

Committee:

Richard D. Miller, Chairperson

Georgios P. Tsoflias

Jennifer A. Roberts

Date approved: _____

Abstract

Attention to specific parameters can minimize inconsistency in source and receiver coupling thereby minimizing changes in spectral characteristics of time-lapse seismic data related to the near surface. This study concludes that the most repeatable Vibroseis source station terrains are firm, unconsolidated sediments that result in 80% shot-to-shot similarity. The least repeatable Vibroseis source station terrains are compacted sediments, resulting in 36% shot-to-shot similarity. Changes in energy containment, transmission, and spectral characteristics of recorded wavefield components occur with repeat shots from downhole projectile sources and appear to be associated with plastic deformation of hole wall sediment. Changes in hole wall sediment conditions with repeat shots has a different effect on surface waves and compressional waves. This observation has potential application to wavefield separation. Acquisition approaches typically used to optimize 2D or 3D high-resolution seismic surveys may reduce repeatability of high-resolution time-lapse data.

Table of Contents

List of Figures

List of Tables

Acknowledgments

I am so thankful for all of the support I have received that has helped me along the way to where I am today. My sincere gratitude goes out to my advisor Rick Miller, for his guidance, patience and support. To my committee members and professors, for beginning my geophysics education and teaching me how much I still have to learn. To everyone in Exploration Services at the Kansas Geological Survey, especially Jianghai Xia, Julian Ivanov, and Brett Wedel for their invaluable assistance in technical and field work. To my fellow students over the years, especially Theresa Rademacker, Jamie Lambrecht, Lindsay Mayer, Daniel Rice, and Joe Kearns, for their assistance and for all the good times we have had.

Above all, I am extremely grateful for my family and friends, who have lovingly endured graduate school right along with me. Mom, Dad, Kara, Brad, and Matt – I love you guys, thanks for everything.

Introduction and Background

Seismic sections or cubes are used to interpret subsurface lithologies and geologic features (Lillie, 1999). For some applications, principal targets are changes in subsurface geology or hydrology that occur over time periods ranging from hours (Birkelo et al., 1987) to years (Raef et al., 2004; Lambrecht and Miller, 2006). A baseline (or background) survey is acquired to estimate initial subsurface conditions. Differences in seismic attributes between the baseline and later monitor surveys are used to interpret net changes in subsurface conditions (Li et al., 2001).

One of the first time-lapse seismic imaging projects was completed by Greaves and Fulp (1987). The goal of the project was to monitor an in-situ combustion enhanced oil recovery process. Acquisition and computer processing were the same for each seismic dataset allowing direct comparisons of many data characteristics. Two amplitude difference volumes were successfully generated from three separate three-dimensional stacked seismic volumes. This study concluded that seismic reflection surveys could be used to successfully monitor enhanced oil recovery processes, and by the mid-1990s time-lapse seismic surveying evolved into a promising technology for oil production management (He et al., 1996; Janson, 2001).

Though time-lapse seismic techniques have been predominantly applied to conventional seismic reflection surveys used for reservoir management (de Waal and Calvert, 2003), time-lapse has been applied to high-resolution seismic reflection surveys for environmental investigations. Birkelo et al. (1987) acquired high-

resolution seismic data over a period of fifteen days to monitor the drawdown of the 2.7 m deep water table during a pumping test. Baker et al. (2000) attempted to monitor submeter seasonal water-table fluctuations over the course of one year. Unfortunately, significant variation in data quality, frequency response, and near-surface conditions inhibited the necessary consistency in data processing and, therefore, interpretation efforts. McKenna et al. (2001) modeled buoyant contaminant flow in water-saturated unconsolidated sand and generated seven synthetic 3D seismic datasets, successfully testing a technique that has potential to monitor groundwater contaminant flow. Lambrecht and Miller (2006) acquired two 3D seismic datasets to monitor dissolution and slumping of beds overlying a salt dissolution sinkhole in Kansas over a period of seven years. Sloan et al., (2007) acquired three 2D seismic profiles one year apart to monitor changes in the top of the saturated zone (TSZ) during, after, and with no pumping from an agricultural irrigation well. Changes were successfully monitored by analyzing amplitude variation with offset (AVO) of the TSZ reflection.

Seismic surveys must be highly repeatable to permit confident extraction of the physical property changes from time-lapse data (Huang et al., 1998; Ebrom et al., 1998). Surveys that lack repeatability will not accurately represent time-lapse anomalies related to subsurface change leading to difficulties interpreting time-lapse data (Ross et al., 1996; Ross and Atlan, 1997; Zamorouev et al., 2006). Many factors may affect the repeatability of high-resolution time-lapse seismic data. Errors in source and receiver positioning (Calvert, 2005), equipment used, ambient noise

conditions, variability in source and receiver coupling (Aritman, 2001), and near-surface changes due to seasonal conditions (Baker et al., 2000) may have a negative impact on repeatability during data acquisition. Standard processing techniques widely used on two- and three-dimensional seismic data can adversely affect time-lapse seismic data during computer processing (Porter-Hirsche and Hirsch, 1998).

Processing techniques have been developed to enhance the repeatability of data that were not acquired with identical acquisition parameters or near surface conditions. Cross-equalization is a technique in which wavelets from the baseline and monitor surveys are estimated and shaped so that reflection data from all monitor surveys match the baseline, thus increasing repeatability (Ross et al., 1996; Rickett and Lumley, 2001). Cross-equalization is considered by some to be a crucial, indispensable step in time-lapse seismic data processing to minimize dissimilarities caused by non-repeatability during acquisition (Ross et al., 1996).

While cross-equalization can improve repeatability by reducing the differences between baseline and monitor surveys, it cannot entirely eliminate differences related to acquisition (Ross and Atlan, 1997). By optimizing repeatability during data acquisition and using a processing approach that maintains repeatability, the actual time-lapse anomalies can be detected on seismic sections.

Purpose

The purpose of this study is to investigate key considerations necessary to optimize repeatability of high-resolution time-lapse seismic data during the acquisition stage. Factors that can affect repeatability in the field include consistency of source coupling, uniformity of energy seal, variability of acquisition geometry, and change in ambient noise conditions. Data for this study were acquired when ambient noise was minimal, and source and receiver stations were either located using a highly accurate real-time kinematic differential global positioning system (RTK DGPS) or remained in place between surveys, to ensure accurate acquisition geometry with each survey. I present data acquired at three locations across the central United States (Figure 1). The first was a 3D survey employing a vibratory source across a large acquisition area spanning numerous terrain types. The latter two surveys employed projectile sources fired into pre-drilled holes in unconsolidated near surface material. I identify changes related to source and/or receiver coupling in each study, quantify seismic changes unrelated to subsurface change, and then recommend acquisition procedures to optimize high-resolution time-lapse seismic surveying.

Part I: Russell County, Kansas

Geologic Setting

A four-dimensional (4D) Vibroseis monitoring survey that was part of the US DOE funded enhanced oil recovery (EOR) program in the Hall-Gurney field in

Figure 1 – Map of study areas. Data for this study were acquired in Russell County, Kansas; Las Cruces, New Mexico; and Lawrence, Kansas.

Russell County, Kansas (Raef et al., 2004) provided data for this study. Time-lapse anomalies from this field were so weak that standard time-lapse analysis techniques were not effective in monitoring this EOR. For the project to meet the proposed objective it was necessary to use parallel progressive blanking, an amplitude envelope 4D horizon attribute that is sensitive to weak time-lapse signatures, to map the movement of carbon dioxide through the field (Raef et al., 2005).

That target of this investigation (Figure 2) was the approximately 900 m deep 3.6 to 6 m thick oomoldic limestone member (Plattsburg) of the Lansing-Kansas City (Raef et al., 2004). These rocks are part of a sequence of Upper Pennsylvanian cyclothems that were deposited as coarse-grained ooid sands on a shallow marine shelf. Exposure to subaerial conditions and meteoric waters has subsequently caused ooid dissolution, resulting in oomoldic grainstones (Watney, 1980). Development of these carbonate-dominated cyclothems was predominantly controlled by sea level (Watney, 1985).

Large land surveys may span a variety of terrains. The acquisition area of a single land survey may contain mountain, desert, gobi, and loess (Qian et al., 2006) or range from open prairie to steep foothill terrain (Beaubouef et al., 2005). Source and receiver stations were located in roads, sand dunes, tilled fields, and pastures in the 4D monitor of Hall-Gurney Field. Soils in the near surface of the survey area (Figure 3) formed from weathering of underlying shale, limestone, and alluvium (Jantz et al., 1982).

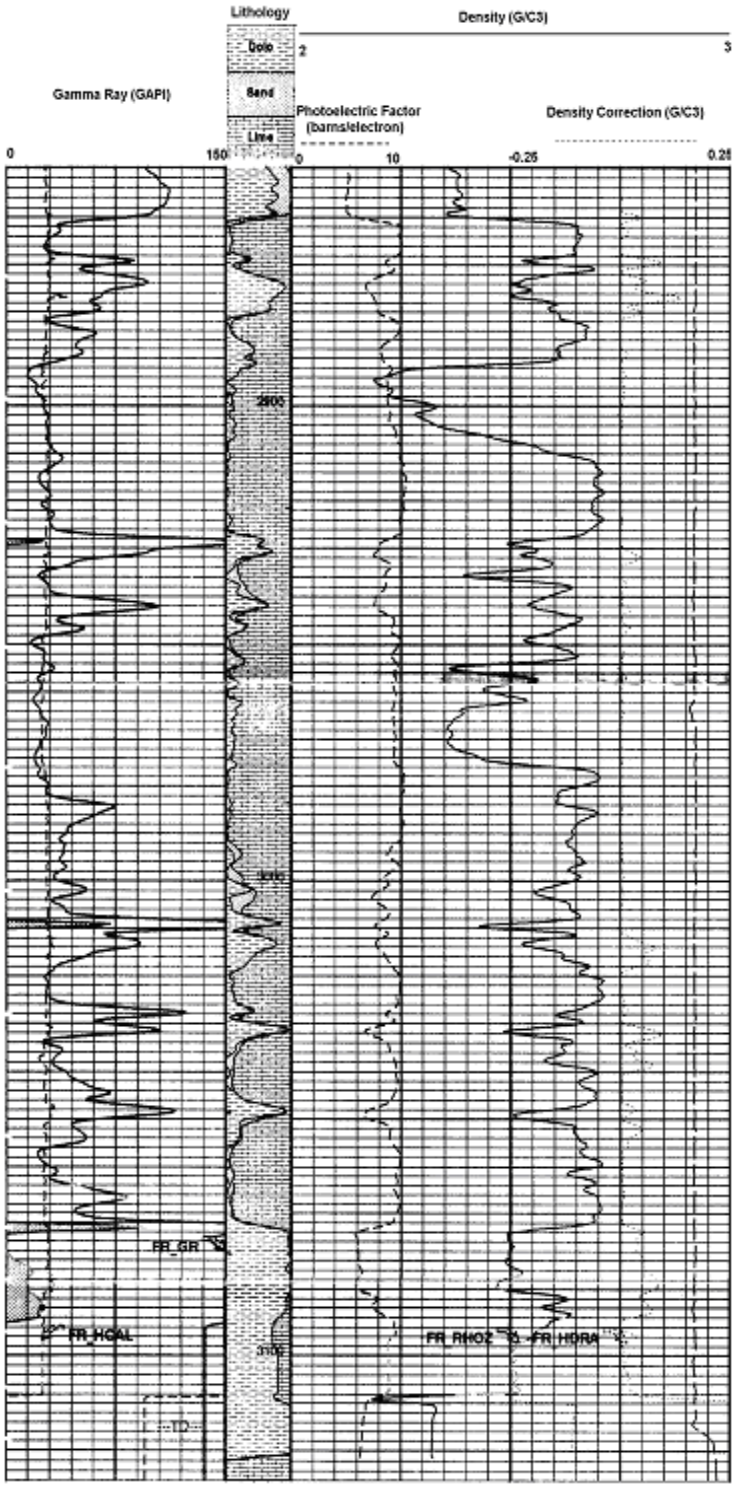

Figure 2 – Logs from Russell County, Kansas. Gamma ray and density logs were acquired October 1, 2000 from well 15-167-23179 in Russell County, Kansas, over Hall-Gurney Field.

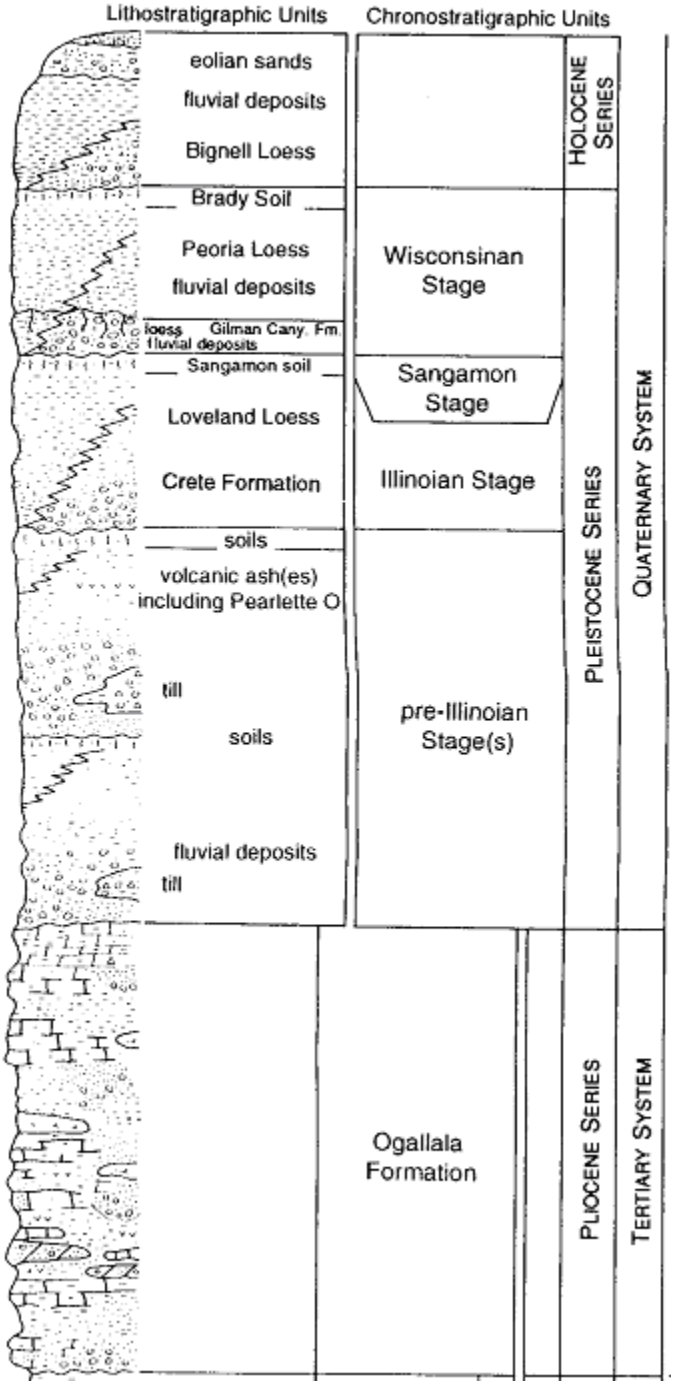

Figure 3 – Near-surface lithology in Russell County, Kansas. From Arbogast and Johnson (1996).

Data Acquisition

The baseline survey for the CO_2 monitoring experiment was acquired in November 2003 and followed by eight monitor surveys, one approximately every four months. Most data were acquired at night to minimize wind noise. The surveys spanned a source area of approximately 3.6 km^2. An IVI Minivib II generated five ten-second linear upsweeps with a frequency range of 20-250 Hz at each source station.

Forty-eight receiver spreads were equally distributed along each of five receiver lines located using a Trimble RTK DGPS. Accuracy requirements of receiver placement were to ensure straight grid lines that did not deviate in line-to-line spacing by more than 0.2 m, and to ensure precise receiver re-deployment. Three Mark Products U2 10-Hz geophones with 14-cm spikes were placed at the point of a half-meter equilateral triangle centered on the receiver station. Each receiver was planted at the base of a hole dug as much as 10 to 15 cm through the sod and into firm soil, thereby ensuring good receiver coupling, reducing the effects of wind noise and reduced resolution due to poor coupling (Hoover and O'Brien, 1980).

Nineteen shot lines with approximately 35 vibration points each and 240 receiver stations distributed along a five-line layout constitute a single patch (Figure 4). Both shot and receiver station spacing was 20 m. Shot lines were separated by 100 m; receiver lines were separated by 200 m. Source progression through this spread was along shot lines when possible. Vibrators were RTK DGPS guided to

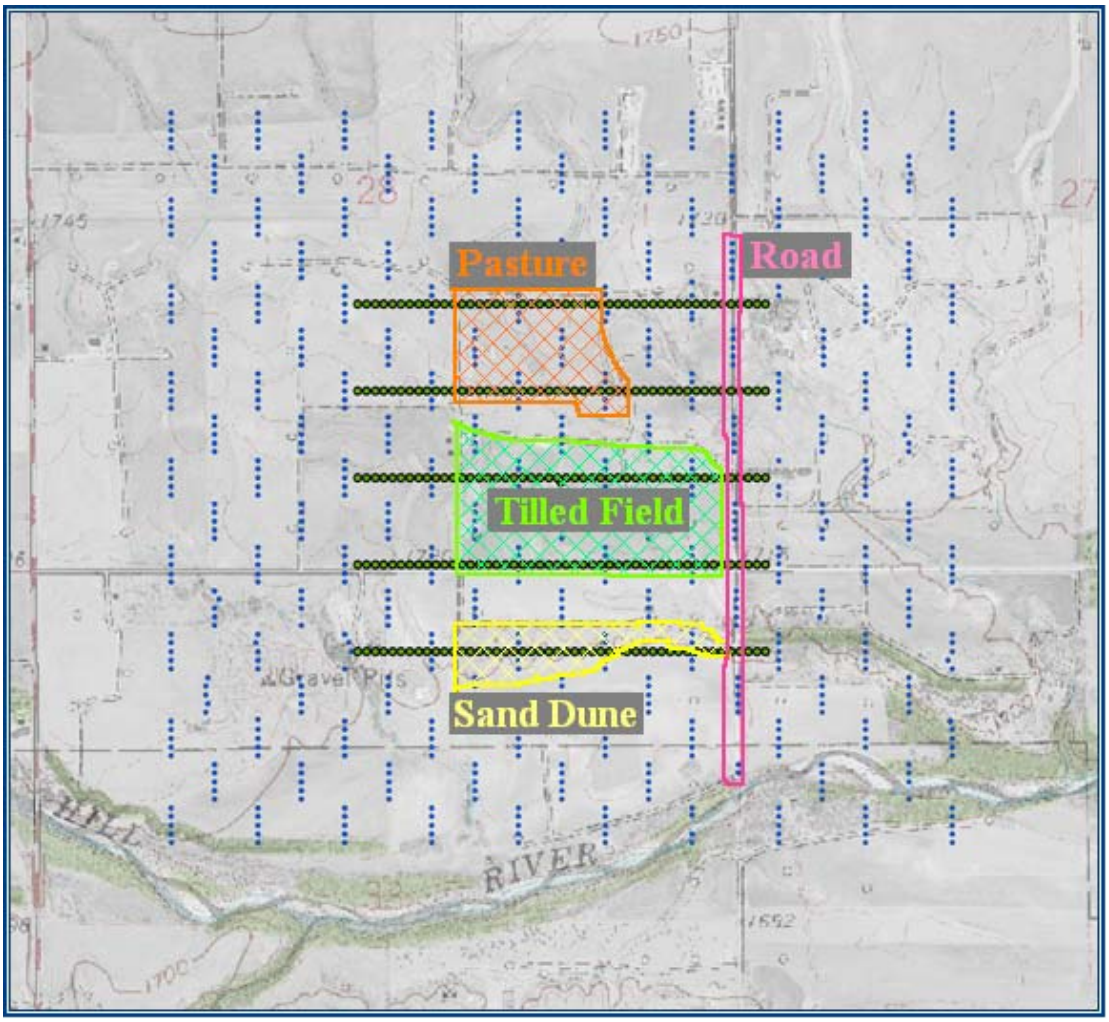

Figure 4 – Field layout in Russell County, Kansas. Source stations are indicated by blue circles; receiver stations are green circles. Examples of the four terrain types are labeled (orange = pasture, light green = tilled field, yellow = sand dune, pink = road).

insure safe operation and optimized repeatability. Five sweeps were recorded uncorrelated and separately at each shot station. The first sweep was designed to compact the ground so that subsequent sweeps were as consistent as possible with minimal plastic deformation of the ground. Only data from the fifth sweep at a station was used for analysis to minimize effects associated with compaction of the near surface beneath the vibrator baseplate.

Analysis of Data

Four unique terrain types were identified in the acquisition area; all contained both source and receiver stations providing a total of sixteen source and receiver terrain combinations. The objective of this case study is to identify the source and receiver terrain combination that provides optimal repeatability of Vibroseis traces both before and after the sweep signal is removed. One receiver station was selected as representative from each of the four terrain types. For each representative receiver station, four corresponding source stations were selected from each terrain type. Because there were seven total time steps (one baseline and six monitor surveys) there were seven traces that were associated with each source and receiver (equivalent traces). These seven traces for each terrain combination were sorted into one gather (Figure 5).

Changes in seismic attributes associated with subsurface change were minimal, and required special processing and analysis to detect (Raef et al., 2005).

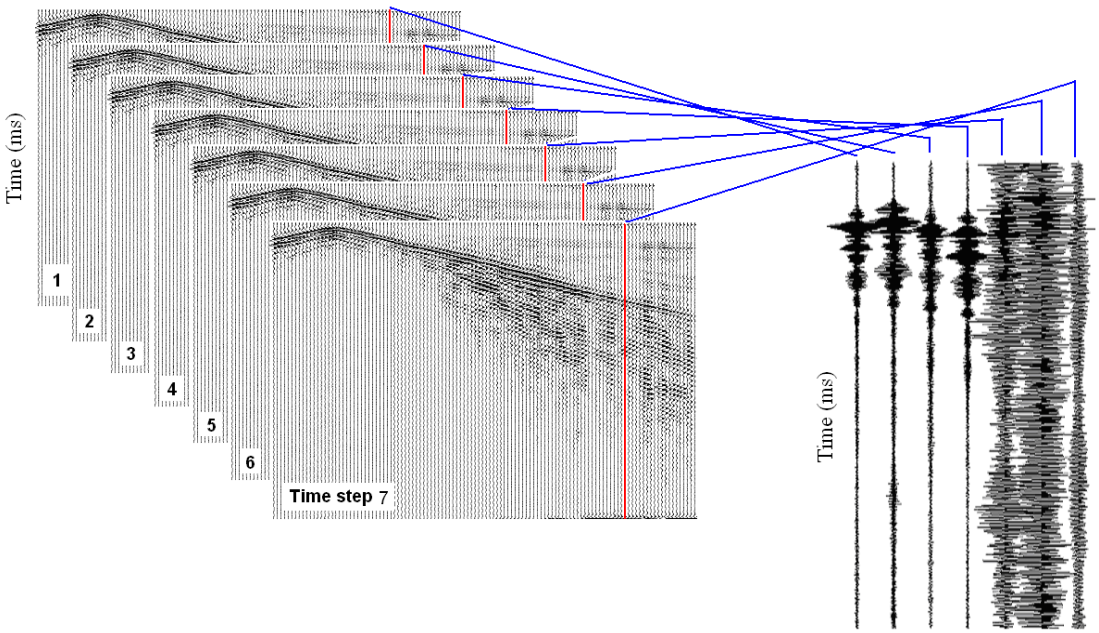

Figure 5 – Equivalent uncorrelated Vibroseis trace gather. Traces associated with a particular source station, recorded by the same receiver were removed from shot gathers and assembled into one gather of equivalent traces. In the ideal case, dissimilarity of equivalent traces should only be the result of subsurface change.

Therefore, because acquisition geometry was accurately duplicated with each time step and all other acquisition parameters were unchanged, differences in equivalent traces are proposed here to be caused by inconsistent source and receiver coupling and seasonal changes associated with terrain type (Vesnaver et al., 2003) such as moisture content (Moussa et al., 2002) and vegetative cover (Anderson, 1953). To determine the similarity of equivalent traces, traces must be time-shifted so that recorded energy (e.g. reflections) arrived at approximately the same time on each trace (Figure 6). The appropriate shift for each monitor trace is assumed to be the shift that results in the maximum correlation coefficient with respect to the baseline. The maximum correlation coefficient of unprocessed Vibroseis traces yields incorrect time shifts that did not shift recorded energy to the same time on equivalent traces. Cross-correlating each trace with a synthetic sweep first, then determining the time shift that resulted in the maximum correlation coefficient results in the correct time shifts. This shift was applied to each unprocessed Vibroseis trace, and the correlation coefficient was calculated for each monitor trace relative to the baseline. The mean and the standard deviation were calculated for the set of correlation coefficients for each terrain combination.

This procedure was repeated for two additional sets of equivalent traces to provide redundant information for each source and receiver terrain combination. Two source and receiver stations with offsets comparable to the offset of the first source and receiver pair were selected for each terrain combination. The appropriate time shift was determined, traces were shifted, and maximum correlation coefficients

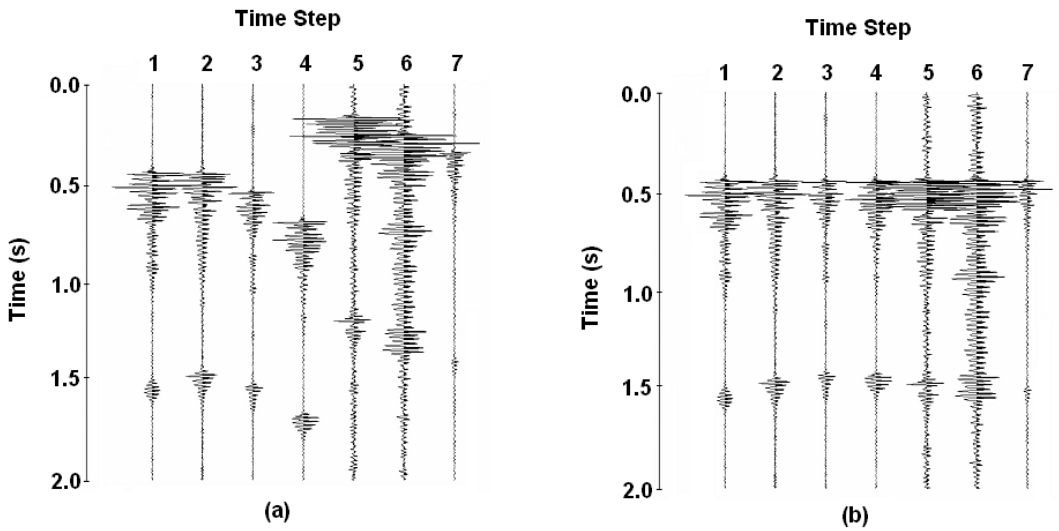

Figure 6 – Shifted equivalent trace gathers. Traces in (a) are the unprocessed traces of Figure 5 cross-correlated with a synthetic sweep, which more closely resemble the seismic trace that would result from convolution of the reflectivity series with a zero-phase wavelet. These traces are shifted (b) so that events have the same two-way traveltime, thus, maximizing the correlation coefficients.

were calculated. The mean (C_i) and standard deviation (σ_i) of correlation coefficients were calculated for each terrain combination. According to Taylor (1997), multiple measurements of the same value (here, mean correlation coefficient) can be used to calculate a single estimate, the weighted average, of that value. Each of the three mean correlation coefficients is weighted (w_i) according to the inverse of the square of the standard deviation:

$$w_i = \frac{1}{\sigma_i^2}$$

The weighted average (C_{avg}) and its uncertainty (σ_{avg}) are:

$$C_{avg} = \frac{\sum_{i=1}^{3} w_i C_i}{\sum_{i=1}^{3} w_i}$$

$$\sigma_{avg} = \frac{1}{\sqrt{\sum_{i=1}^{3} w_i}}$$

The weighted average correlation coefficient was calculated for each terrain combination (Table 1).

Cross-correlation and deconvolution are two techniques used to remove the embedded sweep wavelet from Vibroseis data. Cross-correlation with the vibrator sweep signal was the method used by the inventors of Vibroseis (Crawford et al., 1960) and is the industry standard (Brittle et al., 2001). According to Brittle et al. (2001) the advantage of this method is that it filters unwanted frequencies not contained within the sweep. The disadvantage is that the embedded sweep is

Table 1 – Weighted average correlation coefficients of unprocessed traces. The weighted averages of data from three sets of equivalent traces in each source and receiver terrain combination.

Receiver Terrain	Source Terrain	Correlation	Uncertainty
Dune	Dune	0.32	0.06
Road	Dune	0.13	0.02
Tilled Field	Tilled Field	0.09	0.01
Tilled Field	Dune	0.08	0.02
Pasture	Road	0.07	0.01
Dune	Road	0.06	0.01
Pasture	Dune	0.06	0.01
Road	Road	0.06	0.01
Dune	Pasture	0.05	0.01
Pasture	Tilled Field	0.05	0.01
Road	Pasture	0.05	0.01
Road	Tilled Field	0.05	0.01
Tilled Field	Pasture	0.05	0.01
Pasture	Pasture	0.04	0.01
Tilled Field	Road	0.04	0.01
Dune	Tilled Field	0.03	0.01

removed, and a zero-phase Klauder wavelet is left in its place (Yilmaz, 2001) that can be problematic during processing (Gibson and Larner, 1984). The advantage of deconvolution is that it leaves no residual effects of the sweep and theoretically results in perfect reflectivity. The disadvantage of this method is that it amplifies unwanted nosie (Brittle et al., 2001). To determine the effect each of these techniques has on the repeatability of Vibroseis data, all shifted, unprocessed equivalent traces were first cross-correlated with a synthetic sweep (Figure 6). Average correlation coefficients of cross-correlated monitor survey traces (relative to the associated cross-correlated baseline trace) were calculated for all three gathers of equivalent traces for each terrain combination (Table 2).

The force exerted by the vibrator baseplate on the ground (F_g) is:

$$F_g = M_r a_r + M_b a_b$$

where M_r and a_r are the mass and acceleration of the reaction mass, respectively, and M_b and a_b are the mass and acceleration of the baseplate (Sallas, 1984). The ground force for each trace was calculated by weighted summing of the signals recorded by accelerometers on the baseplate and reaction mass of the vibrator (Figure 7). Vibrator operations during acquisition caused a DC-bias after four seconds, which does not accurately represent the ground force signal and must be corrected through filtering. The calculated ground force signal was corrected prior to deconvolution using two methods: low-cut filtering to remove data components below 0 Hz, and time-variant filtering to insure data at frequencies consistent with the sweep are consistent with the time window (Figure 8).

Table 2 – Weighted average correlation coefficients of cross-correlated traces. The weighted averages of data from three sets of equivalent cross-correlated traces in each source and receiver terrain combination.

Receiver Terrain	Source Terrain	Correlation	Uncertainty
Road	Dune	0.80	0.02
Pasture	Pasture	0.75	0.01
Pasture	Dune	0.64	0.02
Road	Pasture	0.64	0.01
Pasture	Tilled Field	0.62	0.03
Dune	Dune	0.60	0.02
Pasture	Road	0.57	0.04
Tilled Field	Dune	0.55	0.04
Tilled Field	Tilled Field	0.55	0.03
Tilled Field	Pasture	0.53	0.03
Dune	Pasture	0.42	0.03
Road	Road	0.42	0.03
Tilled Field	Road	0.37	0.03
Dune	Road	0.36	0.03
Dune	Tilled Field	0.31	0.04
Road	Tilled Field	0.20	0.02

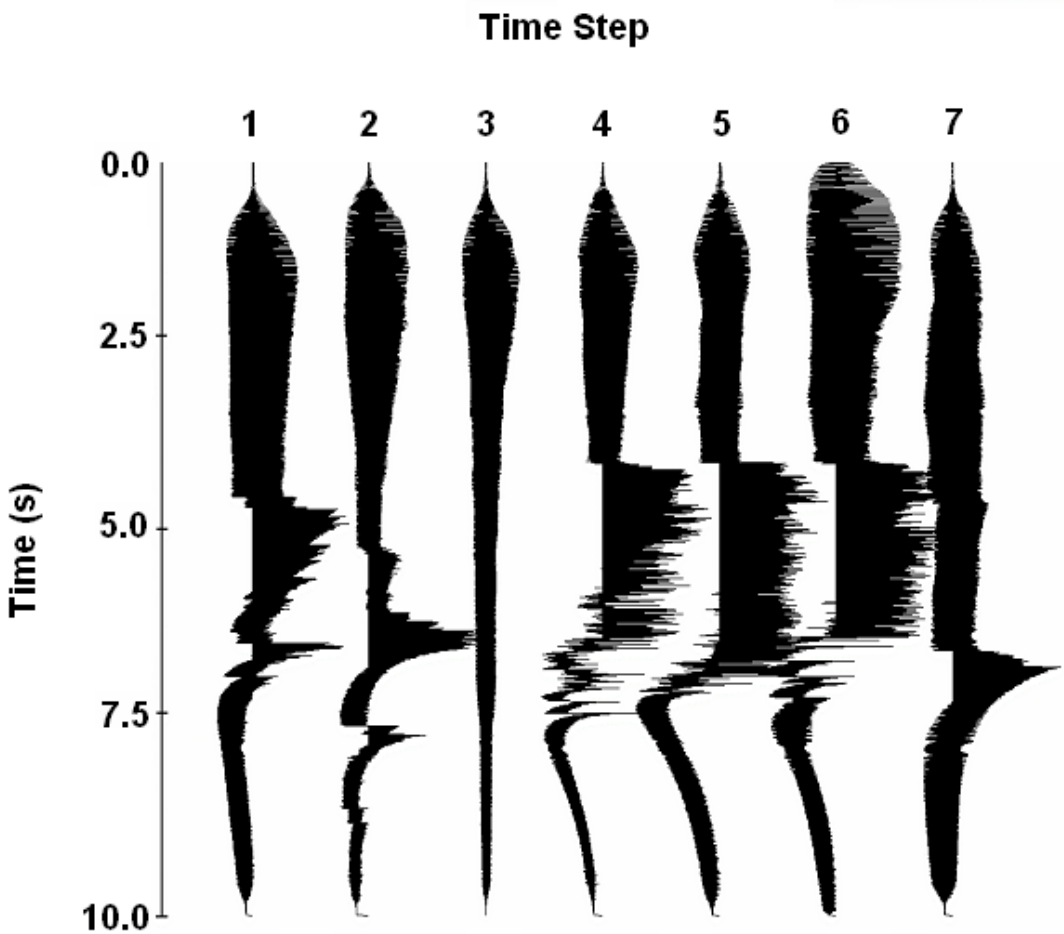

Figure 7 – Measured ground force. The weighted sum of the signals recorded by accelerometers on the reaction mass and baseplate of the vibrator for the equivalent traces in Figure 5. DC bias was caused by slipping (non-uniform mass performance) of the reaction mass begins at approximately 4 s.

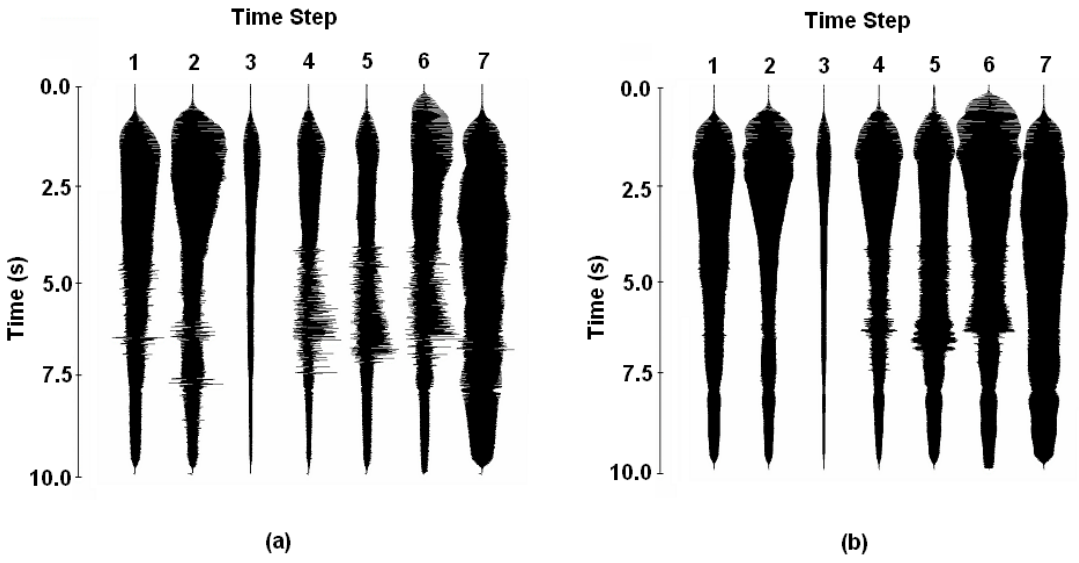

Figure 8 – Corrected ground force. The DC was removed from the weighted sum by two methods: a low-cut filter (a) and a time-variant filter (b).

Unprocessed traces were deconvolved with the low-cut filtered and time-variant filtered ground force signals (Figures 9a and 10a). They were then shifted, and the average correlation coefficients (relative to the baseline) were calculated for each terrain combination. Band-limited spiking deconvolution was then applied (Figures 9b and 10b) to reduce amplified noise and restore amplitudes of frequencies attenuated by the minimum-phase earth filter (Gibson and Larner, 1984; Brittle et al., 2001). Average correlation coefficients for each terrain combination were again calculated (Tables 3 and 4).

Discussion

Roads, pastures, tilled fields, and sand dunes represent uniquely different near-surface settings that affect recorded data differently as a result of surface noise and/or seasonal changes. Roads were compact sediment for rural use, and likely remained unchanged between surveys. Tilled fields, on the other hand, change substantially between seasons; they are loosely tilled prior to planting, and vegetated prior to harvest. Tillage generally increases infiltration of precipitation, which subsequently degrades due to natural reconsolidation (Moussa et al., 2002). Pastures have full vegetative cover year-round that protects the soil from erosion and minimizes runoff and moisture loss by evaporation, and may be used for grazing cattle (Anderson, 1953). Sand dunes are consistently very loose and change with contact, and are calendar time variant (Cox, 1999). Signals recorded from a

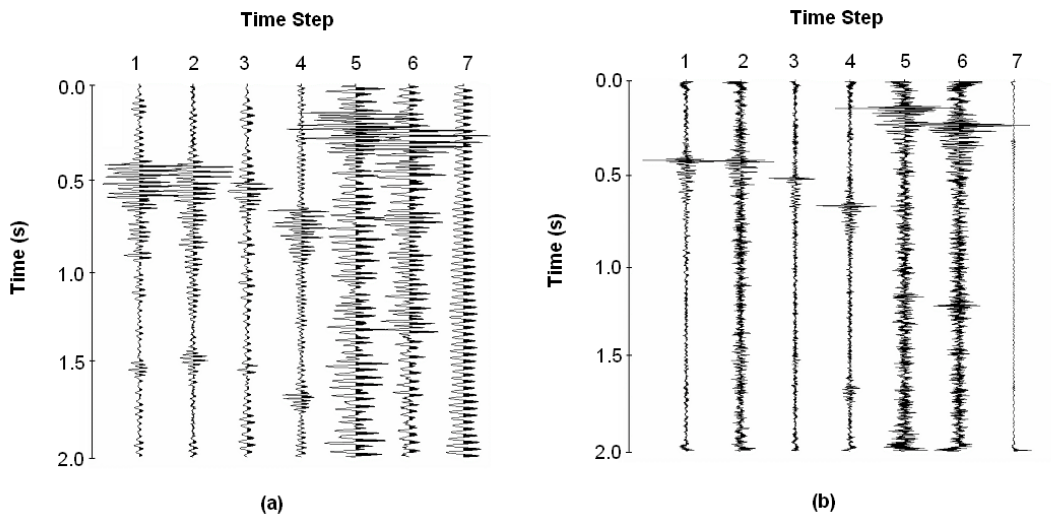

Figure 9 – Equivalent traces deconvolved with the low-cut filtered ground force. These are the unprocessed traces of Figure 5 deconvolved with the low-cut filtered ground force before (a) and after (b) spectral balancing. Correlation coefficients were recorded after shifting for maximum correlation.

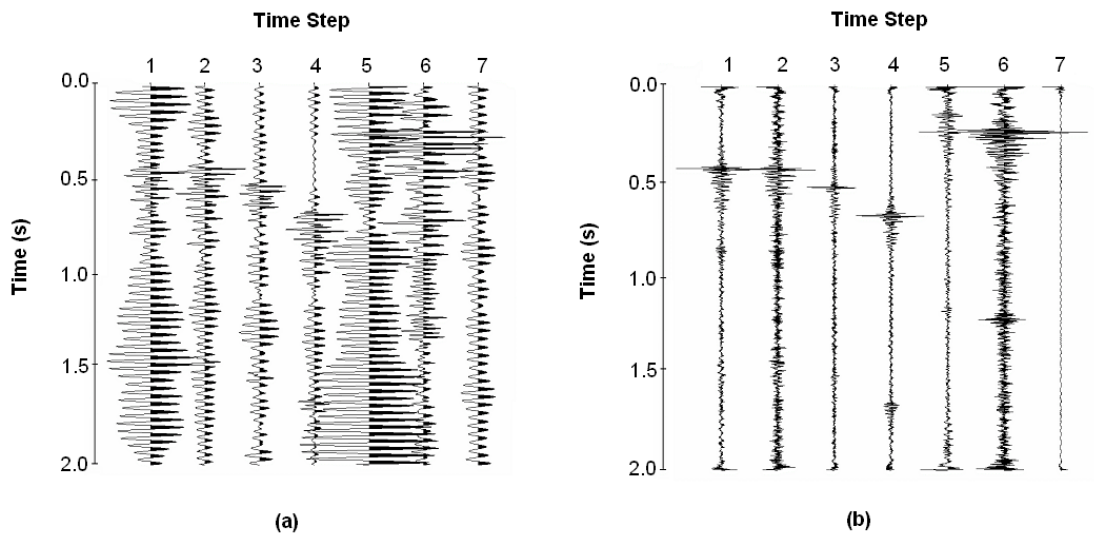

Figure 10 – Equivalent traces deconvolved with the time-variant filtered ground force. These are the unprocessed traces of Figure 5 deconvolved with the low-cut filtered ground force before (a) and after (b) spectral balancing. Correlation coefficients were recorded after shifting for maximum correlation.

Table 3 – Weighted average correlation coefficients of devonvolved traces. The weighted averages of data from three sets of equivalent traces deconvolved with the low-cut filtered ground force in each source and receiver terrain combination. Correlation coefficients before and after applying a spectral balance (SB) are listed.

Receiver Terrain	Source Terrain	Correlation	Uncertainty	Correlation (SB)	Uncertainty
Dune	Dune	0.29	0.03	0.38	0.02
Dune	Pasture	0.14	0.02	0.17	0.01
Dune	Road	0.06	0.01	0.13	0.01
Dune	Tilled Field	0.14	0.03	0.11	0.01
Pasture	Dune	0.27	0.04	0.17	0
Pasture	Pasture	0.22	0.02	0.32	0.01
Pasture	Road	0.11	0.01	0.24	0.01
Pasture	Tilled Field	0.10	0.01	0.22	0.01
Road	Dune	0.26	0.04	0.26	0.01
Road	Pasture	0.20	0.01	0.11	0.01
Road	Road	0.10	0.01	0.19	0.02
Road	Tilled Field	0.09	0.03	0.15	0.02
Tilled Field	Dune	0.26	0.03	0.17	0.02
Tilled Field	Pasture	0.10	0.01	0.22	0.01
Tilled Field	Road	0.10	0.01	0.12	0.02
Tilled Field	Tilled Field	0.13	0.04	0.14	0.01

Table 4 – Weighted average correlation coefficients of devonvolved traces. The weighted averages of data from three sets of equivalent traces deconvolved with the time-variant filtered ground force in each source and receiver terrain combination. Correlation coefficients before and after applying a spectral balance (SB) are listed.

Receiver Terrain	Source Terrain	Correlation	Uncertainty	Correlation (SB)	Uncertainty
Dune	Dune	0.13	0.02	0.23	0.03
Dune	Pasture	0.12	0.02	0.15	0.01
Dune	Road	0.15	0.05	0.15	0.01
Dune	Tilled Field	0.17	0.01	0.19	0.02
Pasture	Dune	0.14	0.02	0.22	0.04
Pasture	Pasture	0.17	0.02	0.17	0.03
Pasture	Road	0.18	0.02	0.14	0.02
Pasture	Tilled Field	0.19	0.03	0.2	0.03
Road	Dune	0.12	0.02	0.15	0.03
Road	Pasture	0.2	0.02	0.18	0.02
Road	Road	0.13	0.01	0.12	0.02
Road	Tilled Field	0.16	0.04	0.04	0.01
Tilled Field	Dune	0.13	0.02	0.15	0.02
Tilled Field	Pasture	0.15	0.02	0.12	0.02
Tilled Field	Road	0.11	0.01	0.13	0.02
Tilled Field	Tilled Field	0.16	0.03	0.13	0.02

geophone and generated from a vibratory source in these terrains are all affected differently with seasonal and surface noise conditions (Figure 11).

Ideally, data recorded for a specific source and receiver pair would be identical each time the receiver recorded data from that source. However, changes in noise, equipment, and near-surface conditions have the most profound effects on recorded data. Because noise conditions were minimal, equipment were deployed using RTK DGPS, and changes in wavelet characteristics associated with subsurface changes are extremely small at Hall-Gurney Field, source wavelet variability from one survey to the next is likely due to changes in the near-surface conditions in each terrain. A trace from the baseline survey should theoretically have a correlation coefficient of 1.0 when compared to equivalent traces on subsequent monitor surveys if repeatability between surveys was perfect. In practice, however, correlation coefficients for unprocessed traces were small. Average correlation coefficients for data at all shot and receiver terrain combinations is 0.08. That means there is only an 8% similarity between equivalent traces; conceptually, it is difficult to consider them to be the same wavelet.

There appears to be a connection between source terrain and correlation coefficients of unprocessed Vibroseis traces. In general, the largest correlation coefficients are for source stations located in the sand dunes. This is not surprising considering the problem of harmonic distortion is more severe on rigid surfaces (Schrodt, 1987; Reust, 1995). Because unprocessed signals are most repeatable when the vibrator is in a sand dune, the most deformable surface, it appears likely that

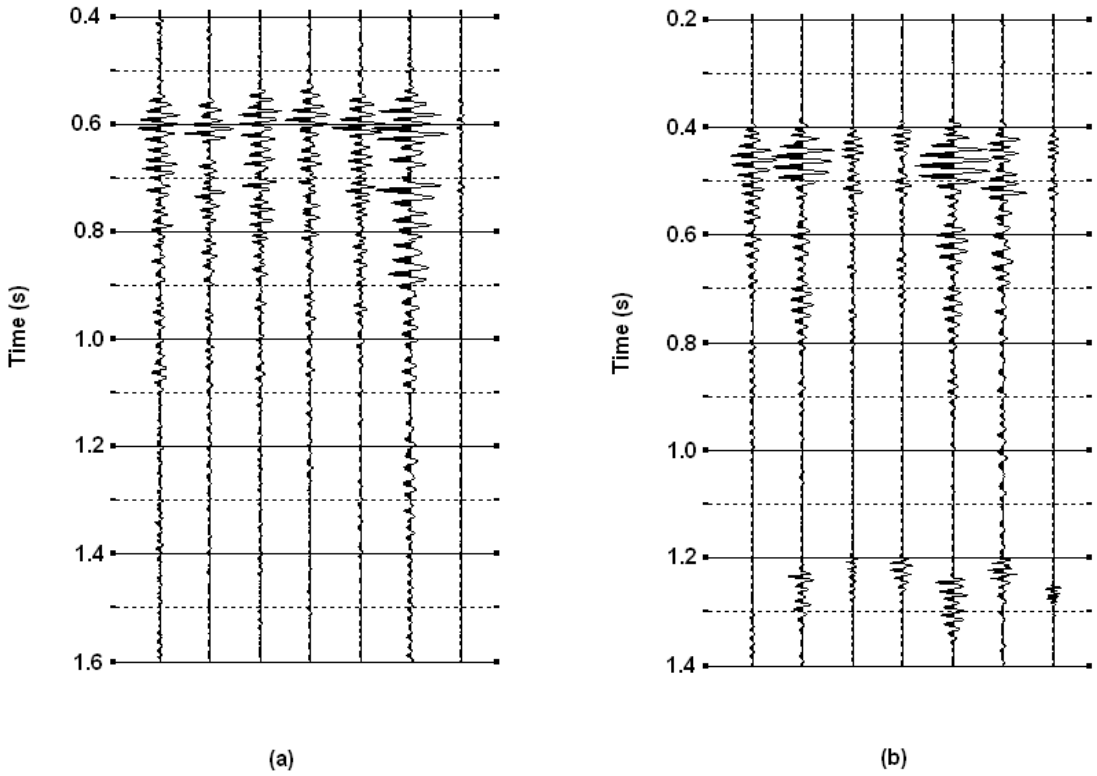

Figure 11 – Equivalent trace gathers from different terrains. Equivalent traces generated when the source was in a sand dune and the receiver was in a pasture (a), and a road (b).

harmonic distortion is a contributor to non-repeatability of unprocessed Vibroseis data in this study.

Average correlation coefficient of equivalent Vibroseis traces is significantly improved after cross-correlation with a synthetic sweep. The average correlation coefficient of Vibroseis traces is 0.52 after cross-correlation. There appears to be a connection between correlation coefficients and source and receiver terrains. With regards to receiver terrain, the largest correlation coefficients are associated with receivers in pastures and roads. These terrains undergo the least change of all the terrain types, and receivers have excellent coupling in both roads and pastures when vegetation is cleared and geophones are planted in firm soil. The lowest correlation coefficients are associated with receivers in sand dunes and tilled fields, which are the least consistent of the four terrain types. Receivers have poor coupling in sand dunes due to their unconsolidated, loose nature, and receiver coupling changes in tilled fields depending upon the season and type of crop.

With regards to source terrain, the largest correlation coefficients of Vibroseis traces after cross-correlation with a synthetic sweep are associated with source stations in sand dunes and pastures. The largest correlation coefficients are associated with source stations in sand dunes and pastures. Sand dunes provide a loose surface that allows for good source coupling and, thus, minimizes harmonic distortion. Pastures change minimally throughout the seasons and have a moderately loose surface. The smallest correlation coefficients are associated with source stations in roads and tilled fields. Roads, while they do not change seasonally, are

extremely rigid surfaces that subject the vibrator baseplate to decoupling from the ground surface, causing harmonic distortion of the sweep signal. Tilled fields, like pastures, are moderately loose, but undergo significant seasonal changes that affect repeatability of the source signal.

No terrain combination responded better to deconvolution with the filtered ground force than to cross-correlation with a synthetic sweep. However, relative observations of least optimal and most ideal source and receiver terrains with deconvolved data are similar to observations made for cross-correlated data. Higher correlation coefficients result from receivers in pastures and sources in sand dunes or pastures. The lowest correlation coefficients result from receivers in sand dunes, and sources in roads and tilled fields.

Conclusions

Equivalent uncorrelated Vibroseis shot records maintain very little similarity during different time steps, with correlation coefficients of only 0.8. Cross-correlating traces with a synthetic sweep significantly improves similarity, more so than deconvolution with the measured ground force. The greatest correlation coefficients of cross-correlated traces are for receivers that are in pastures and roads and sources in sand dunes and pastures. The lowest correlation coefficients are for receivers in sand dunes and tilled fields, and sources in roads and tilled fields.

To optimize repeatability during acquisition, this study found that the field layout should be designed with receivers planted in a firm near-surface allowing

optimal receiver coupling, and source stations should focus on surfaces with perennial vegetation and minimal or no human traffic. By minimizing change in recorded signal between surveys associated with terrain, the repeatability of time-lapse seismic data can be maximized during the acquisition stage.

Part II: Las Cruces, New Mexico

Geologic Setting

Data acquired near Las Cruces, New Mexico, as part of a joint study between the US Army Corps of Engineers and Kansas Geological Survey were designed to further investigate the use of seismic methods as a tool for interrogating earthen levees. To simulate flood conditions, an earthen dam was constructed in the floodplain and against the levee using sediment scraped from the unconsolidated floodplain, and water pumped from the Rio Grande at a rate consistent with model flood conditions. As a part of this project, a two-dimensional (2D) seismic line was deployed in the floodplain parallel to the levee, dam and river. The target of this investigation was the shallow water table. The objective of the profile was to investigate possible changes in reflectivity due to changes in sediment saturation. Because data were acquired along the line multiple times, changes in source coupling and therefore any special equalization steps needed during processing had to be determined.

The recent geologic history and resulting present-day landscape around Las Cruces, New Mexico, focuses around the late Tertiary and Quaternary periods when

the Rio Grande rift was active (Mack, 1997). Extensional forces caused faulting that defines the local north-south trending mountain ranges and adjacent sedimentary basins, which control the course of the Rio Grande (Keller and Cather, 1994). Today, the Rio Grande runs near Las Cruces where it empties into the Gulf of Mexico. A geotechnical engineering study carried out at the site prior to our survey includes boring data suggesting that, in general, the near surface is comprised mostly of unconsolidated silt, sand, gravel, and some clayey layers down to at least 14 m where the borings reached their planned depth (Figure 12). The water table is 1.5 to 3 m beneath ground surface (Esquivel, 2005).

Data Acquisition

The receiver line was in the floodplain and ran parallel to the levee between the river and the dam berm (Figure 13). The line was approximately 7 m from the base of the dam and extended nearly its entire length. Seismic receivers were two Mark Products 40-Hz geophones with receiver stations separated by 30 cm. Source station spacing was 2.5 m, with an off-line offset of 1.2 m. The 30-06 source was fired into pre-drilled holes. Firing downhole reduces the air-coupled wave amplitude, and takes advantage of the exhaust gases in the production of a source wavelet. In most settings, containing the "air blast" results in a greater dominant frequency, larger

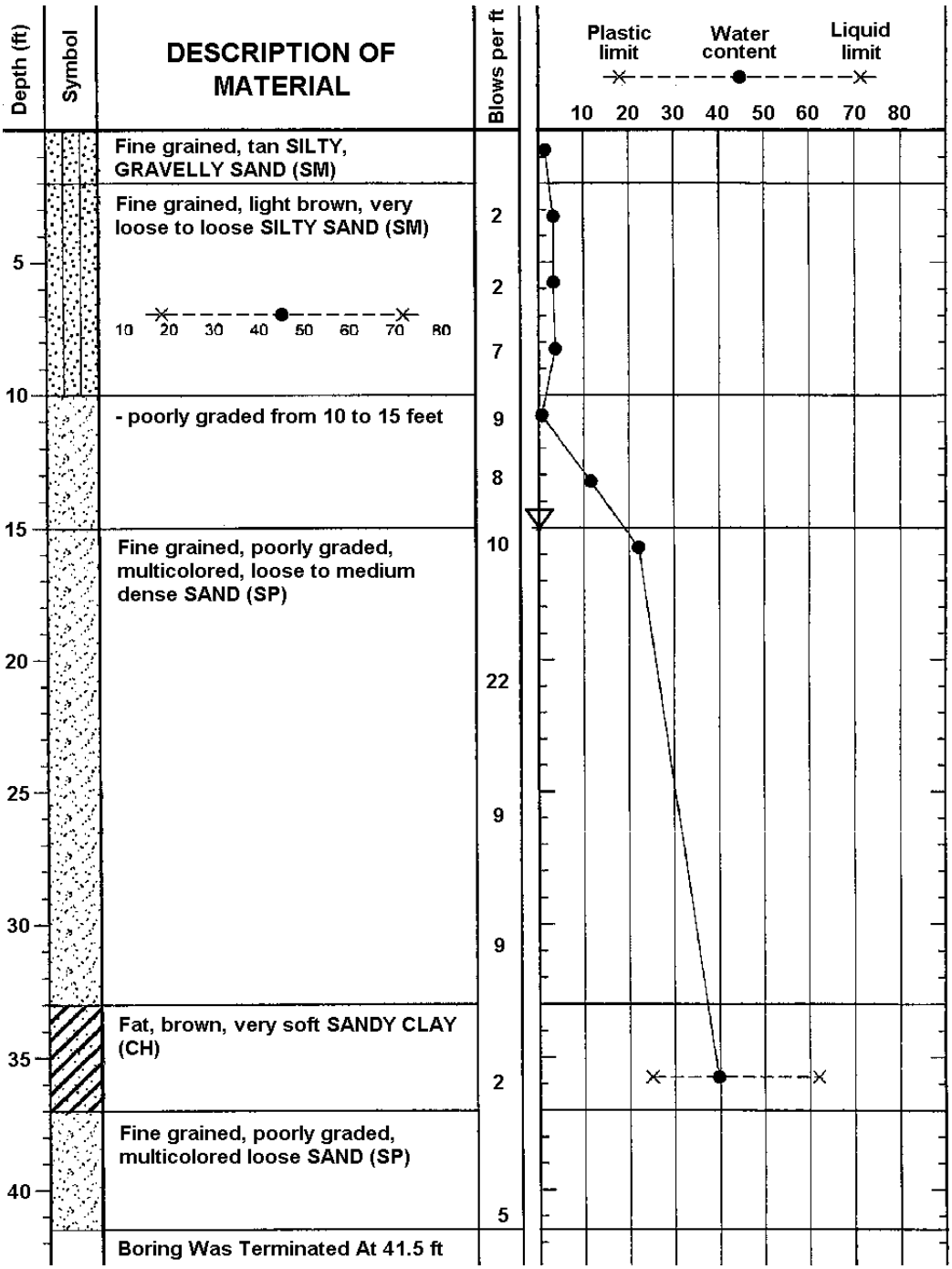

Figure 12 – Near-surface lithology at Las Cruces site. This profile details the near-surface sediment at the site near Las Cruces, New Mexico. It was provided by a geotechnical engineering study carried out at the site prior to our time-lapse survey (Esquivel, 2005).

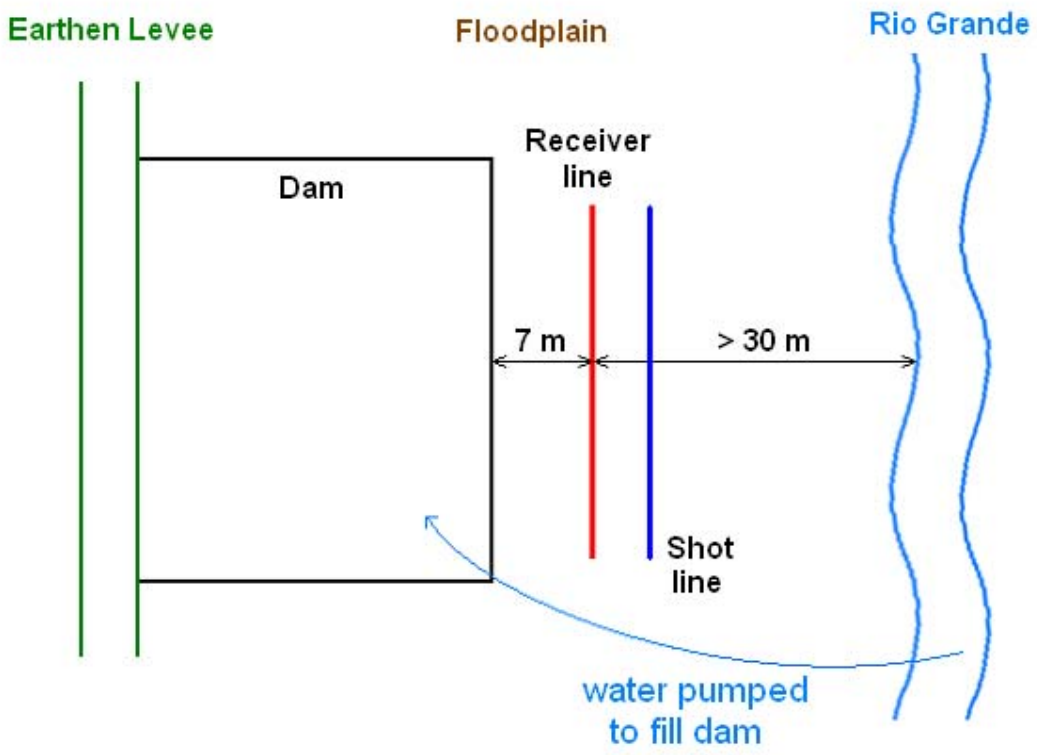

Figure 13 – Field layout in Las Cruces, New Mexico. A single line of receivers ran parallel to the dam in the floodplain. Water was pumped into the pond from the Rio Grand between time steps.

bandwidth and increased signal-to-noise ratio on seismic shot records (Steeples et al., 1987). An approximately 30 cm piece of PVC pipe was placed in the drilled holes and water poured down each hole to saturate the holes and surrounding sediment prior to firing the source.

A baseline survey was acquired at 1:00 PM on September 14, 2005, just prior to the start of water being pumped continuously into the pond. After the pump was temporarily switched off following four hours of operation (to reduce noise), the first monitor survey data were acquired. Water was poured downhole prior to each repeat survey to maximize coupling and minimize shot to shot variability (Miller et al., 2007; Jefferson et al., 1998). This procedure was repeated for each of the eight monitor surveys that spanned thirty-six hours.

Analysis of Data

When a projectile seismic source is fired downhole, both the projectile and the exhaust gases contribute to recorded data (Steeples et al., 1987). The exhaust gases expand due to change in volume relative to the barrel, and a pressure wave travels in the hole. Energy seal refers to how well the pressure wave is contained in the source hole. Source coupling for these types of sources is a measure of how efficiently the pressure wave is transmitted across the air-sediment interface at the hole wall and propagates as seismic energy in the subsurface. The objective of this case study is to characterize changes in energy seal through analysis of the air-coupled wave amplitude, characterize changes in source coupling through analysis of reflection

amplitudes, and examine changes in the entire recorded wavefield caused by repeat shots in the same source hole.

Representative amounts of all components of the wavefield were evident and distinguishable for analysis, with minimal ambient noise recorded on shot gathers from shot stations 993, 1001, 1009, and 1017. To quantitatively analyze how the air-coupled wave amplitude changed from one survey to the next, everything except the air-coupled wave was muted from the set of representative shot gathers after application of a 100 to 500 Hz bandpass filter. The unmuted energy on each trace was transformed into the frequency domain. An amplitude spectrum was calculated for every trace. The amplitude of each frequency on all the traces was averaged together, resulting in an average amplitude spectrum of the shot gather (henceforth, referred to simply as "amplitude spectrum"). Two dominant frequencies were evident in the air-coupled wave packet. The sum of the average amplitudes of these dominant frequencies was calculated for each time step (Figure 14).

To determine how reflection amplitudes were affected by repeated use of the same source hole, everything except the reflection whose zero-offset two-way traveltime is 55 ms was surgically muted from the set of representative shot gathers of each time step. Amplitude spectra were calculated for each selected shot gather; the dominant frequency and its associated absolute amplitude were recorded and plotted (Figure 15).

To determine how significantly the total recorded wavefield changed with repeated shots, a single representative trace (receiver station 1120) was selected from

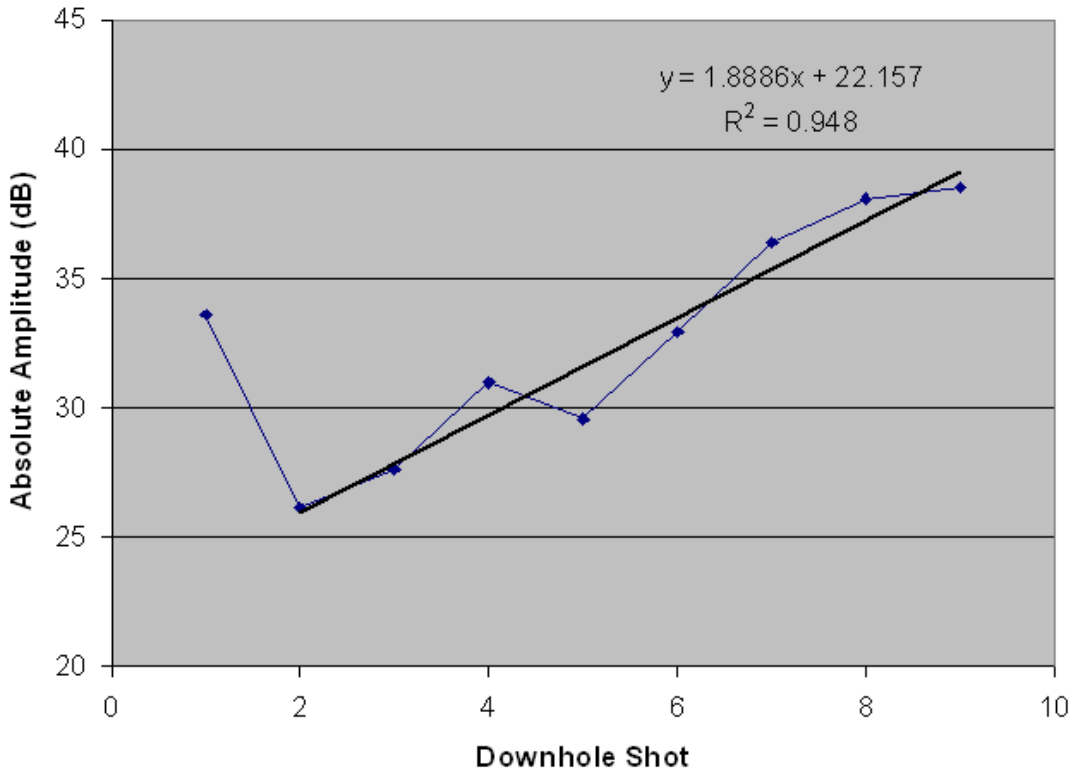

Figure 14 – Average air-coupled wave amplitude. There is a 57% decrease in average amplitude after one shot was fired downhole, followed by a nearly linear increase throughout the remaining time steps.

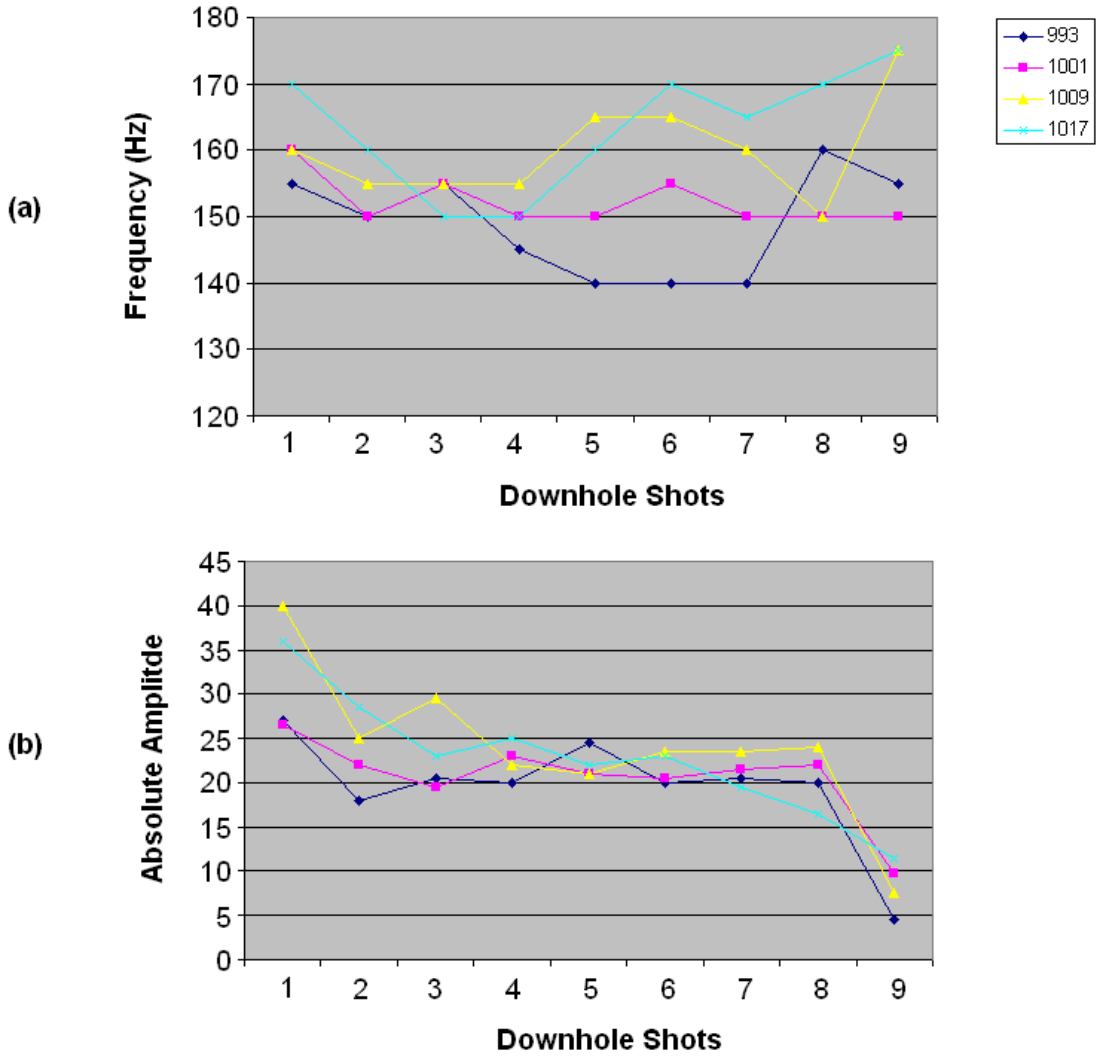

Figure 15 – Average reflection spectral characteristics. Dominant frequency (a) and associated amplitude (b) of the 55 ms reflection event recorded on four shot gathers from each time step.

a representative unprocessed shot gather (source station 1017) from each time step. These traces were extracted and resorted into an equivalent trace gather (Figure 16). Correlation coefficients were determined for all traces with respect to each time step (first, with respect to the baseline; then, with respect to the second time step; etc.). This procedure was repeated for equivalent traces from four additional receivers at stations 1037, 1063, 1075, and 1100 (Figure 17).

Qualitative inspection of equivalent trace gathers indicates that there is a change in ground roll arrival time on equivalent traces. To determine whether or not this change is caused by a change in velocity, dispersion curves were generated and phase velocities calculated for a particular shot gather (source station 1001) from each time step (Figure 18).

Discussion

The 59% decrease in air-coupled wave amplitude from 45,000 to 20,000 (-7.96 dB) between the baseline and first monitor survey is a dramatic change that adversely affects the repeatability of the surveys. After the second shot the average air-coupled wave amplitude increases nearly linearly at a rate of approximately 2 dB per time step. This change suggests improved seal between the gun and hole. It is reasonable to suggest that this effect is the result of hole conditioning by the first shot fired into the source hole. Subsequent increases in the air-coupled wave amplitude suggest a decreasing quality in the source-to-hole seal throughout the remaining eight shots. This leads to the recommendation that, to optimize data acquisition in this

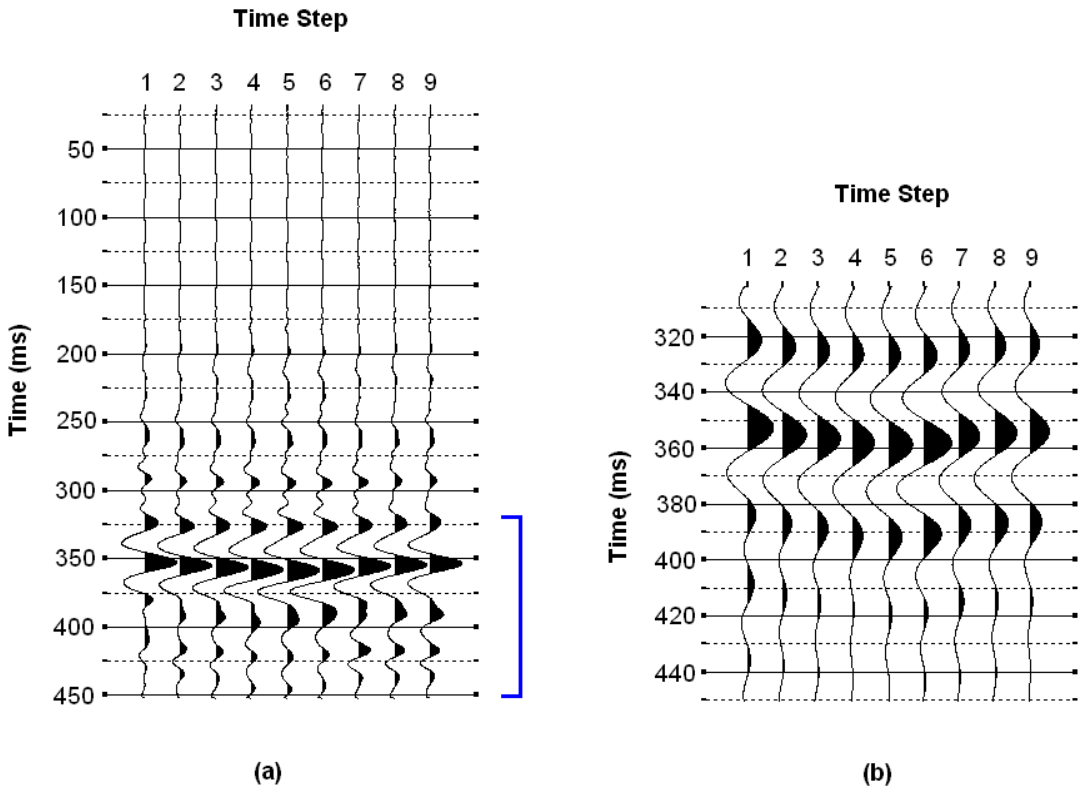

Figure 16 – Equivalent seismic trace gather. The traces in (a) correspond to source station 1017 and receiver station 1120. The blue bracket contains recorded ground roll energy and is magnified in (b) to more clearly see the changing arrival time.

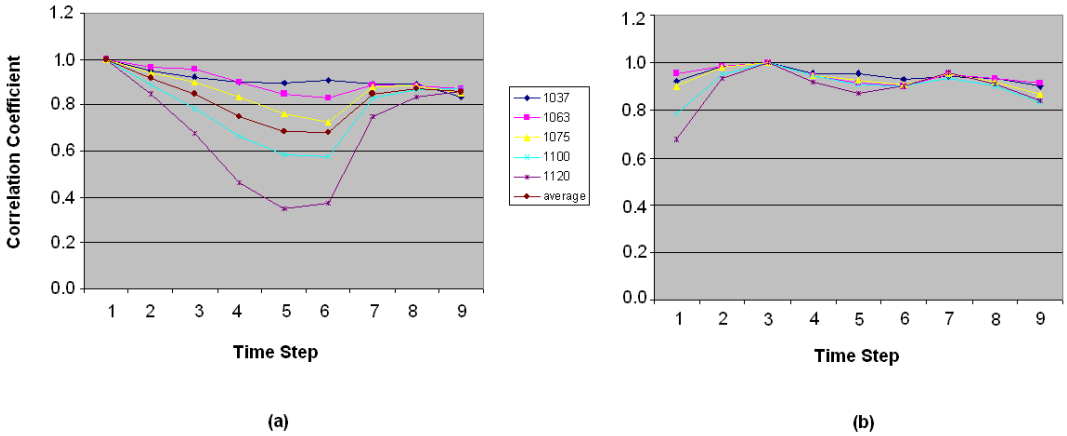

Figure 17 – Correlation coefficients of equivalent seismic trace gather. Correlation coefficients of equivalent traces with different source-receiver offsets with respect to the baseline (a) and with respect to the third time step (b).

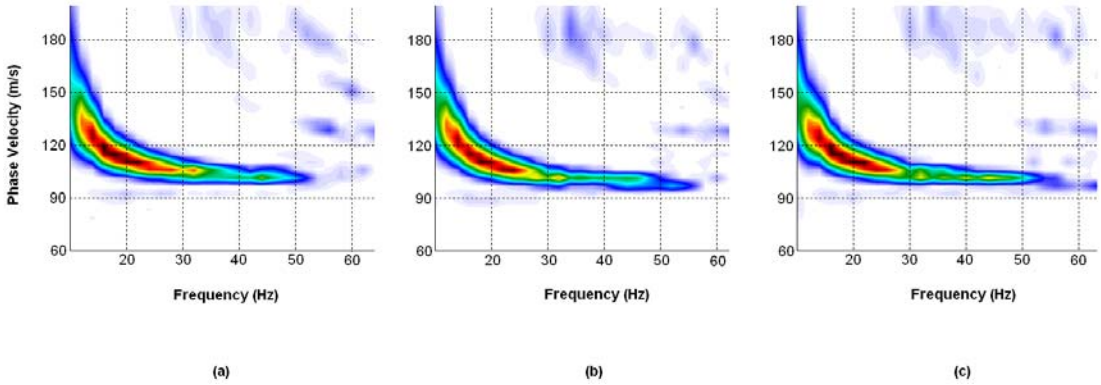

Figure 18 – Equivalent dispersion curves. These curves were generated from unprocessed equivalent shot gathers from station 1001 during the first (a), fifth (b) and ninth (c) time steps. Phase velocity was constant throughout the time-lapse survey.

fluvial setting using a downhole projectile source (specifically a 30-06) a wet pre-drilled source hole requires one downhole shot delivered before data are acquired to condition the hole and maximize the seal. On the sixth shot downhole, the seal had deteriorated to the point the air-coupled wave amplitude was near that observed on the first shot.

Reflection amplitudes were largest for wavelets recorded during the baseline survey (Figure 15b). Subsequent to the first downhole shot, reflection amplitudes remained on average approximately 30% below the baseline survey reflection amplitudes until the ninth downhole shot. On the ninth downhole shot, reflection amplitudes decreased on average by 60%. This suggests that the greatest source coupling occurred during the first downhole shot, with source coupling remaining fairly consistent for the next seven shots after which another significant decrease occurred with the ninth shot. Consistency is vital for high-quality time-lapse seismic data (Huang et al., 1998). Therefore, even though the largest reflection amplitudes are observed on the first shot record, the second through eighth time steps have reflection characteristics that are more consistent and repeatable.

Representative traces selected from shot gathers recorded at the same source station for each repeat survey correlate best with equivalent traces from the third time step (Figure 17*b*) rather than the baseline (Figure 17*a*). Traces from the third time step correlating the best with all shot gathers from a particular hole suggests that a significant change occurs in the source signature or energy transfer after firing the

second shot. This change continues with subsequent shots, but is most consistent for all surveys with the third shot.

An apparent increase of 1 to 5 ms in ground roll traveltime appears dependant on source-to-receiver distance and the number of shots fired downhole (Figure 16). For a set of traces from shot gathers acquired at the same source station ground roll traveltime consistently increases through each of the first five shots, and then consistently decreased for the last four shots. Dispersion curves generated for each survey indicate that ground roll phase velocity was consistent for all nine surveys. The traveltime increase therefore must be the result of a change in hole wall sediment conditions as a function of number of shots fired downhole.

Conclusions

Amplitude analysis of the air-coupled and reflection wavelets, and examination of correlation coefficients of equivalent traces was the basis for characterizing changes in repeat shots of an impulsive source in a fluvial depositional setting. The air-coupled wave amplitude decreases significantly after the first downhole shot, indicating an improved ground to surface seal. Reflection amplitudes decrease significantly after the first downhole shot, indicating a decrease in source coupling of body wave energy. Reflection amplitude remained approximately the same for the seven subsequent shots, indicating a stable, consistent source coupling. Correlation coefficients of equivalent traces from different shots are a maximum for the third shot. Therefore, to optimize repeatability, the source should be fired twice

in each hole to adequately condition the hole prior to acquiring time-lapse seismic data. A traveltime shift was observed in the ground roll while its phase velocity remained constant, and no traveltime shift was observed for body waves or the air-coupled wave. These observations suggest that plastic deformation of the hole wall sediment affected the propagation of ground roll.

Part III: Lawrence, Kansas

Geologic Setting

Data for the third part of this study were acquired in Lawrence, Kansas, near the Kansas Geological Survey on the University of Kansas west campus. These data are not associated with another project, but were acquired solely to simulate a time-lapse survey in this near-surface setting.

This site was selected because it produced high-quality seismic data collected during a past survey by Knapp (1988). The targets of this investigation were the two prominent reflections recorded by Knapp (1988), the tops of the Haskell Limestone and Stoner Limestone at depths of approximately 56 m and greater than 92 m (Figure 19), respectively (O'Conner, 1960). The Haskell and Stoner Limestones are members of the Upper Pennsylvanian carbonates. These rocks were deposited on a gently tilted shallow marine shelf that was subject to rhythmic flooding and subaerial exposure controlled by the eustatic sea level (Watney, 1985; Watney, 1980). In the near surface of the site (Figure 20) are Martin and Vinland soils that formed

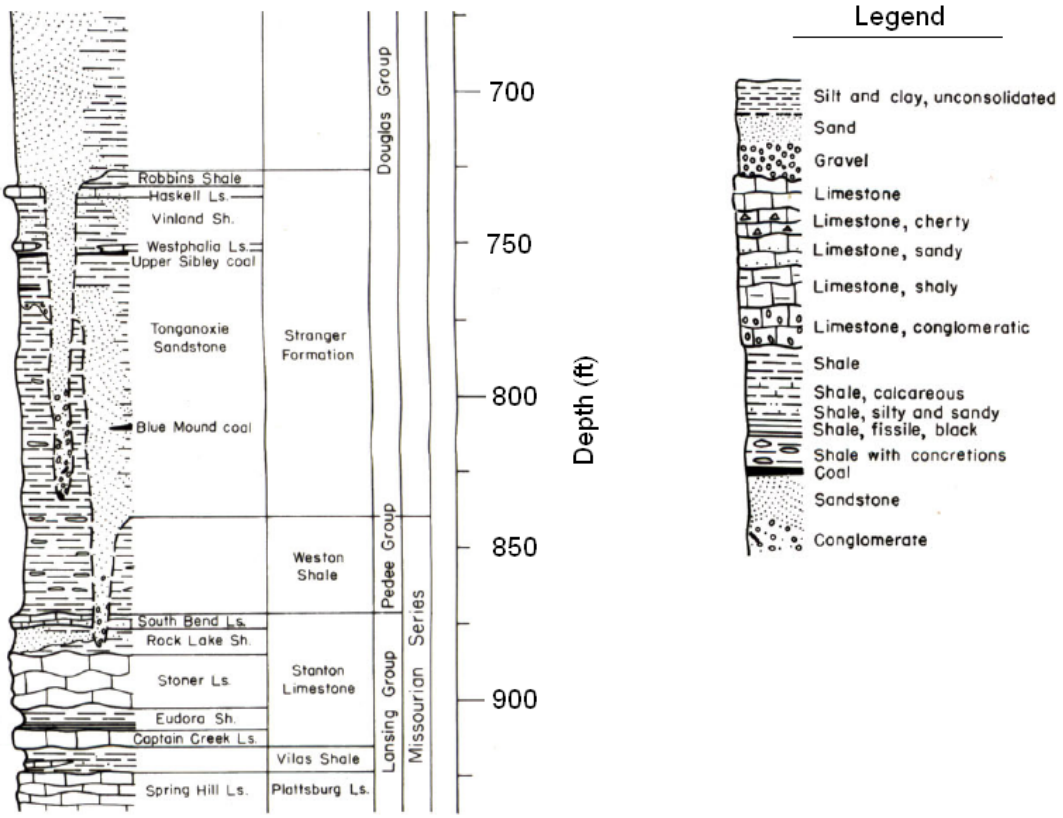

Figure 19 - Lithology of Douglas County, Kansas. Vertical profile of the deeper lithology in Douglas County (O'Conner, 1960).

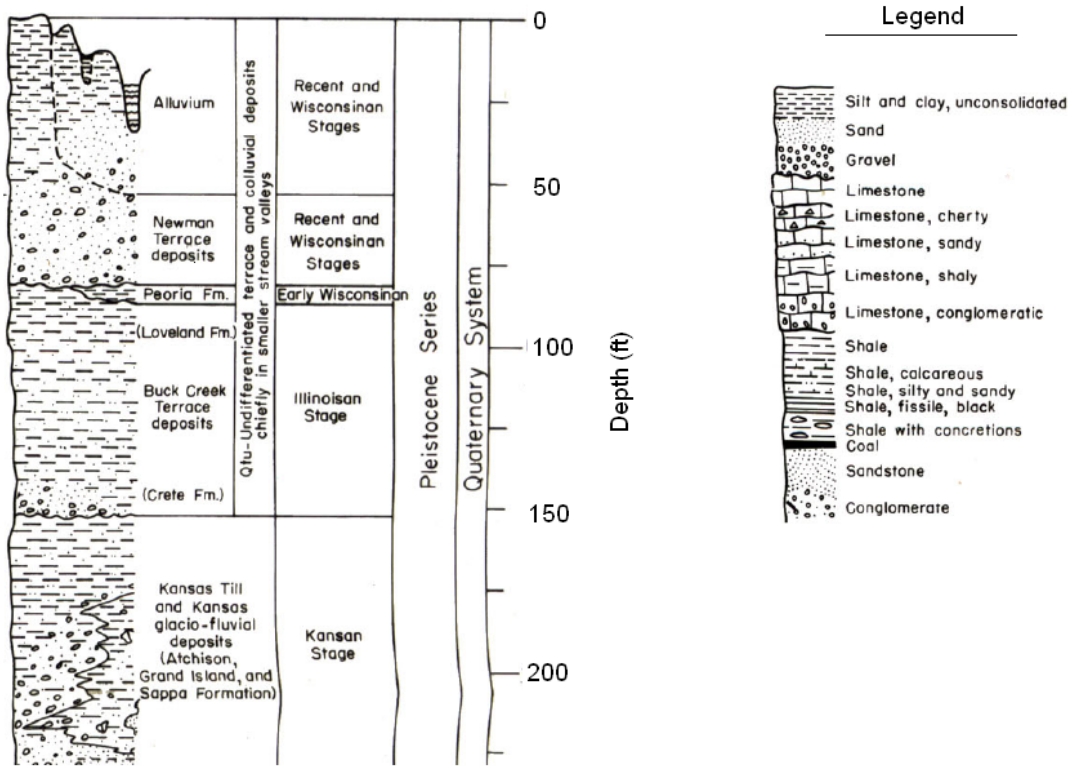

Figure 20 – Near-surface lithology of Douglas County, Kansas. Vertical profile of the near surface in Douglas County (O'Conner, 1960).

from weathered shale (Dickey et al., 1977) and are rich in smectite (Schulmeister et al., 2003).

Data Acquisition

Data for the study at the Kansas Geological Survey (Figure 21) were acquired at night in an open field south of the complex and west of a major US highway. Recording at night was done specifically to avoid traffic noise. A fixed line of sixty receivers was oriented approximately east-west and perpendicular to nearby US HWY 59. Each of the sixty seismic receiver stations were separated by 0.6 m and occupied by two Mark Products 40-Hz geophones with 1.2 m station spacing. Vegetation at each receiver station was cleared, and receivers were planted in firm soil. Two impulsive sources, modified .50-caliber and 30-06 downhole rifles (Miller et al., 1986; Steeples et al., 1987; Miller et al., 1992; Miller et al., 1994) were used along separate, parallel source lines. The .50-caliber source line was parallel to the receiver line and approximately 4.9 m to the north. The 30-06 source line was parallel to the receiver line and approximately 1.2 m to the north. One-meter deep, dry source holes were pre-drilled every 3.7 m along both source lines. This sparse source station spacing was selected because this study does not require large fold.

This particular study was designed to evaluate source consistency and any associated change in attributes related to repeated shots in this dry, weathered shale near surface, especially as the subsequent effects affected time-lapse signal analysis techniques. The procedure required ten shots be fired and recorded separately once

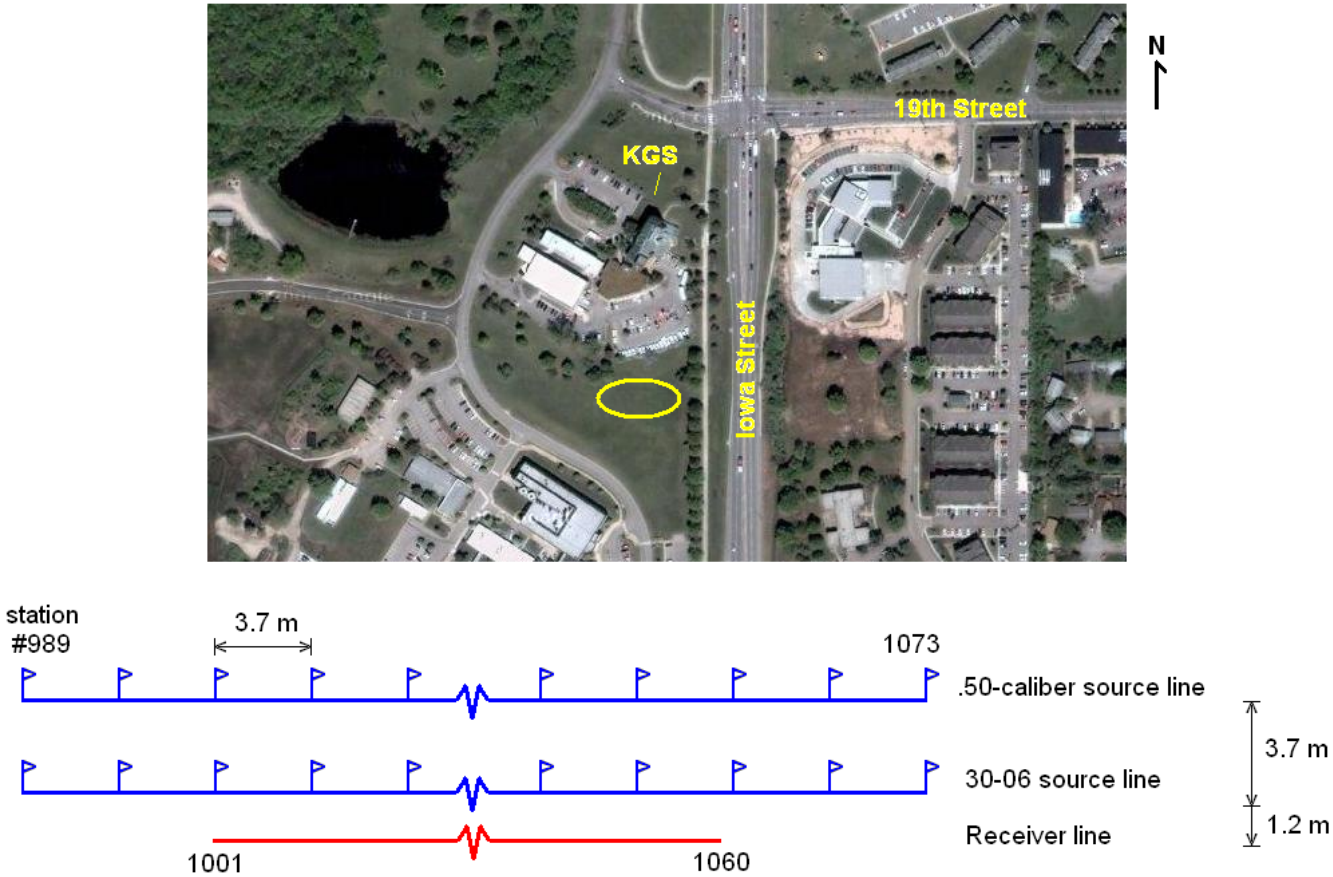

Figure 21 – Field layout in Lawrence, Kansas. Field site is circled in yellow on the satellite image. Image courtesy of Google maps.

the source was placed in a source hole. All sixty recording channels were live for each shot. At the conclusion of the acquisition phase, ten sixty-channel shot gathers had been recorded at each source station for both sources.

Analysis of Data

The objective of this case study is to examine changes in the spectral characteristics (dominant frequency, amplitude, and useable bandwidth) and arrival times of recorded components of the wavefield associated with repeat shots in the same source hole, and evaluate source wavelet consistency throughout the time-lapse survey. To do so, a set of representative shot gathers with sufficient amplitudes of ground roll, guided waves, first arrival, air-coupled wave, and reflections had to be selected for analysis for both the .50-caliber and 30-06 projectile sources.

A shallow, abrupt velocity contrast at the base of the uppermost layer that can be characterized as having a velocity gradient will produce dispersive ground roll and guided waves (Sheriff, 2002; Robertsson et al., 1995). Both wave types appear on shot gathers acquired with both the .50-caliber and 30-06 projectile sources. The ground roll and guided waves have large amplitudes and low dominant frequencies relative to reflections, air-coupled waves, and ambient noise (Figure 22). Due to their dispersive nature they are difficult to remove with *f-K* filtering without distorting signal from reflections (Yilmaz, 2001; Karsli and Bayrak, 2003). However, their

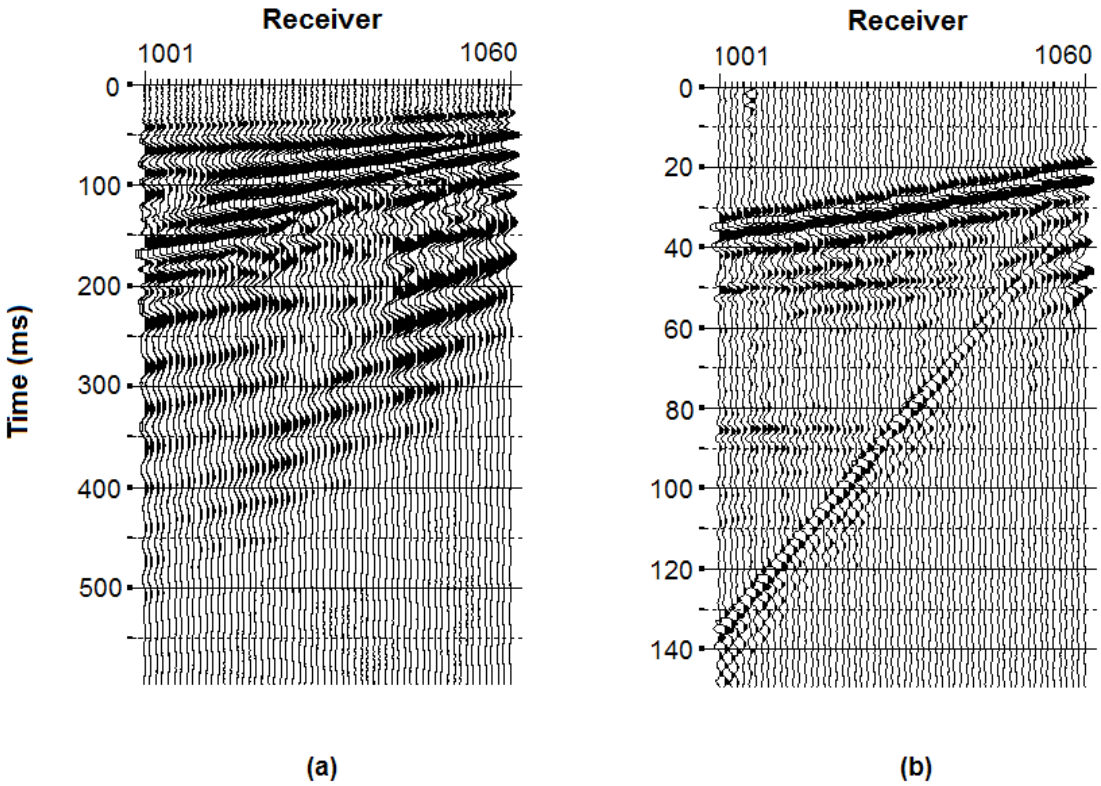

Figure 22 – Example of dominant low-frequency energy. Shot gather corresponding to station 1073, time step 5. Ground roll and guided wave energy are very high amplitude on unprocessed shot gathers (a). After application of a low-cut frequency filter, both ground roll and guided waves were suppressed, revealing the lower-amplitude reflections and air-coupled wave (b), indicative of the band-limited nature of ground roll and guided waves (Robertsson et al., 1995).

comparatively low dominant frequency (Figure 23) may make use of a low-cut filter effective in attenuating their amplitudes.

A tapered low-cut filter with 0% and 100% corners at 100 and 200 Hz, respectively, successfully attenuated the ground roll and guided waves to reveal reflections on shot gathers acquired with the .50-caliber projectile source (Figure 22*b*). However, filtering did not effectively attenuate these waves on shot gathers acquired using the 30-06 source (Figure 24). Therefore, data acquired with the 30-06 projectile source were unable to be used for analysis. Henceforth, only data acquired with the .50-caliber source are discussed. Representative amounts of all components of the wavefield were evident and distinguishable for analysis on shot gathers from shot stations 1055, 1061, 1067, and 1073.

To isolate how the ground roll dominant frequency, and amplitude changed during each time step, all energy outside of the window in which ground roll arrived was surgically muted in the time domain from the set of representative shot gathers (Figure 25). Amplitude spectra (Figure 26) were generated for equivalent shot gathers for each time step. The change in dominant frequency and associated amplitude were evaluated for each shot gather (Table 5). This procedure was repeated for recorded guided wave energy.

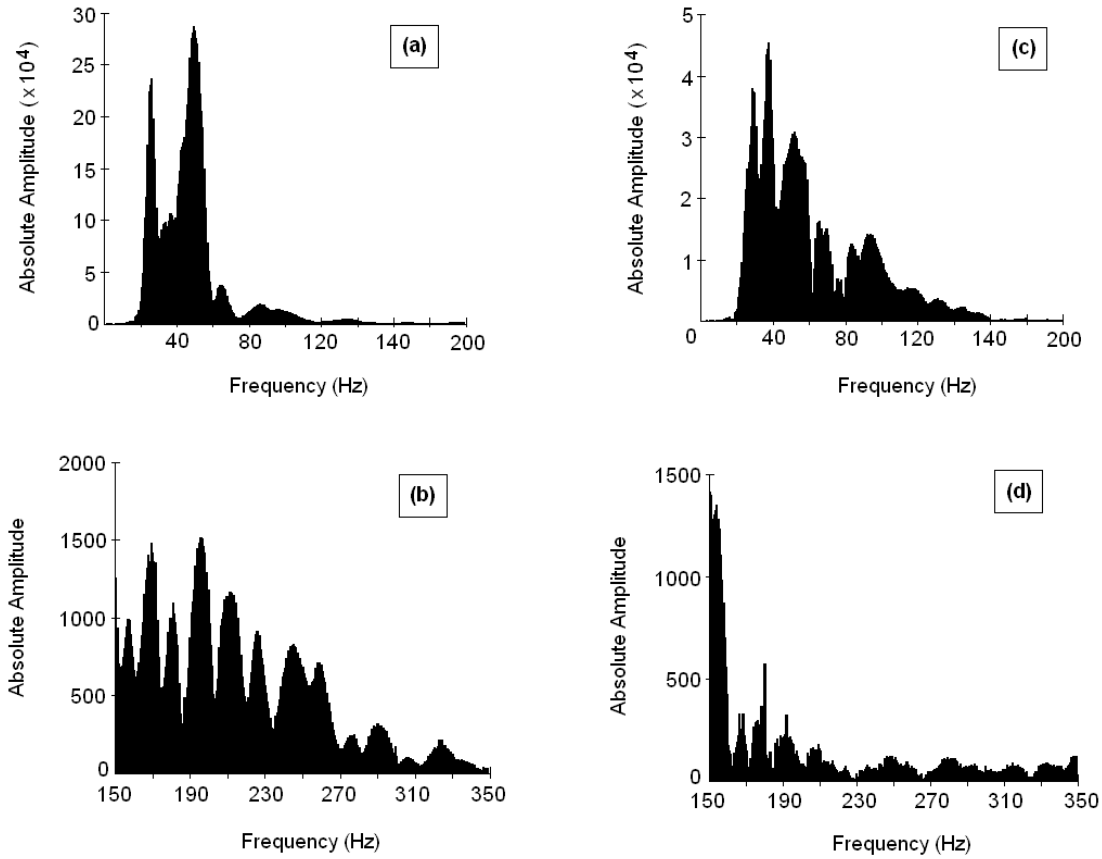

Figure 23 – .50-caliber and 30-06 amplitude spectra. Generated from shot gathers corresponding to shot station 1073 during the first time step. The low frequencies produced by the .50-caliber projectile source (a) were two orders of magnitude larger than the higher frequencies (b). Low frequencies produced by the 30-06 projectile source (c) were one order of magnitude larger than the high frequencies (d).

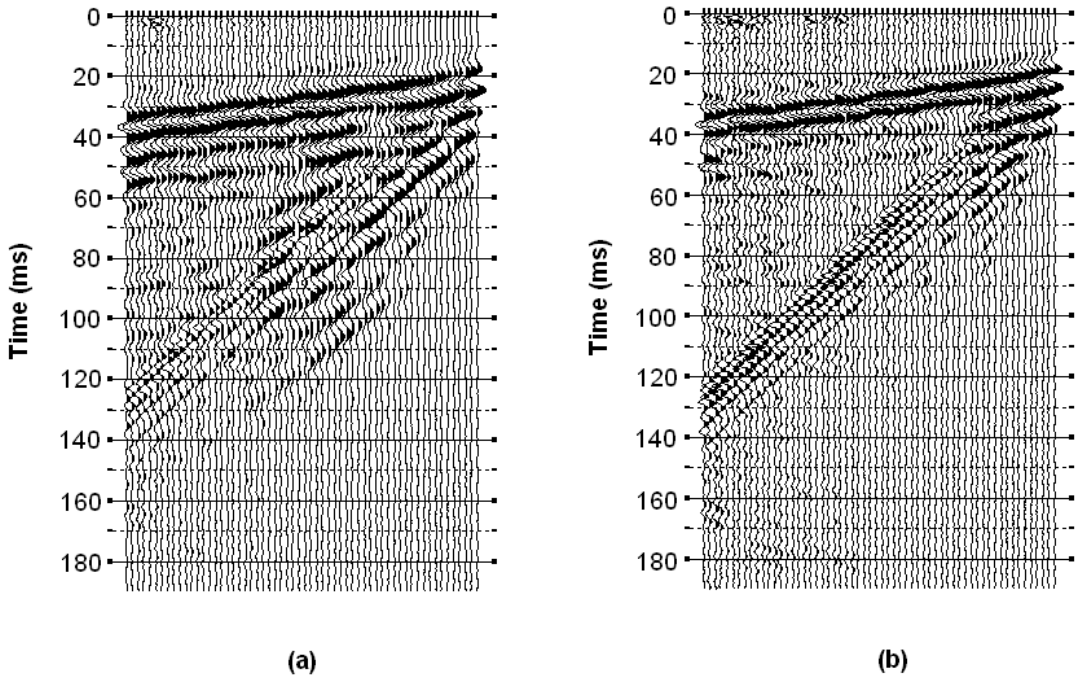

Figure 24 – Low-cut filtered 30-06 data. (a) The shot gather from source station 1067 using the 30-06 projectile source after application of a 65-150 Hz low-cut filter. (b) The shot gather from source station 1067 after application of a 100-200 Hz low-cut filter. The reflection seen in Figure 22 should be apparent. Filters sufficient for attenuating ground roll and guided waves produced with a 30-06 projectile source also attenuate reflections.

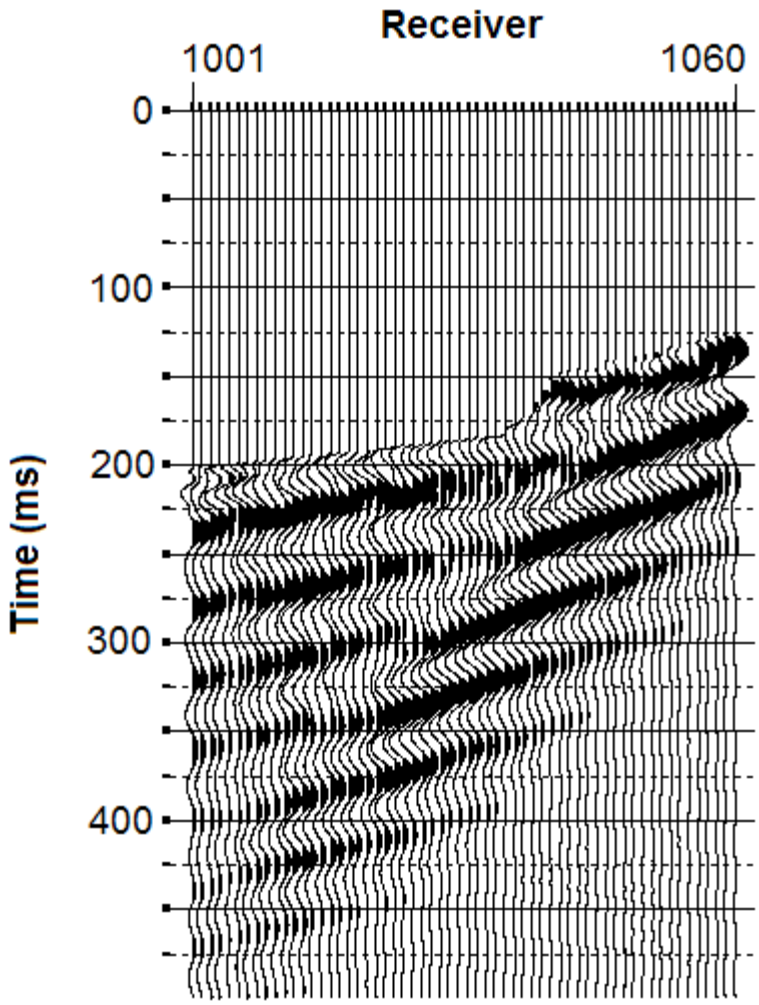

Figure 25 – Ground roll remaining after mute. This is what remains of the unprocessed shot gather from the fifth time step at source station 1073 after muting all signal outside the window in which ground roll arrives.

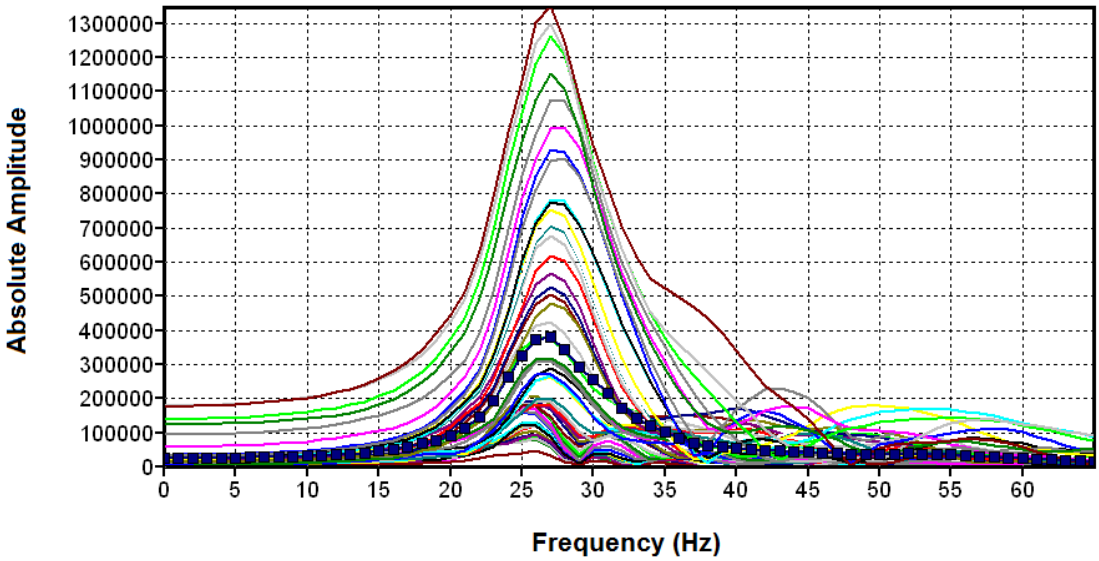

Figure 26 – Amplitude spectra of ground roll. Amplitude spectrum of the unprocessed shot gather from the fifth time step at source station 1073. Amplitude spectra were generated for each time step, and data were compared to determine what changes due to time-lapse surveying took place between time steps.

Table 5 - Full wavefield spectral data. Dominant frequency and associated amplitude of ground roll, guided waves, first arrival, and the Haskell and Stoner Limestone (L.S.) reflections from shot records at source station 1073 during each time step. Air-coupled wave amplitude is the total amplitude over all frequencies from station 1067 shot records.

		Shot 1	Shot 2	Shot 3	Shot 4	Shot 5	Shot 6	Shot 7	Shot 8	Shot 9	Shot 10
Ground Roll	Frequency (Hz)	27	27	27	27	27	27	27	27	27	27
	Amplitude	380000	233000	233000	242000	240000	240000	247000	252000	260000	272000
Guided Wave	Frequency (Hz)	49	49	48	48	48	48	48	48	48	48
	Amplitude	263000	173000	171000	170000	172000	167000	164000	173000	166500	172500
First Arrival	Frequency (Hz)	177	174	175	180	178	186	181	180	180	175
	Amplitude	3165	2680	1940	1345	1065	990	1090	1130	1090	1175
Haskell L.S. Reflection	Frequency (Hz)	187	181	187	195	202	206	203	201	180	193
	Amplitude	3520	2870	2980	3195	2780	3110	2760	3150	2740	3000
Stoner L.S. Reflection	Frequency (Hz)	186	198	198	205	208	216	211	211	208	203
	Amplitude	4240	3090	2445	2370	2145	2750	2470	2440	2325	2470
Airwave	Amplitude	5249751	704855	690214	795251	949392	806549	775621	812818	706985	710053

Using a similar procedure as described above, the first arrival was isolated on the low-cut filtered representative shot gathers. The dominant frequency and associated amplitude determined from amplitude spectra were recorded (Table 5). This procedure was repeated for the Haskell Limestone reflection, Stoner Limestone reflection, and air-coupled wave.

To determine the usable bandwidth of the ground roll (bandwidth of ground roll amplitude above ambient noise amplitude), the amplitude spectrum of ambient noise arriving prior to the first arrival was calculated for both the unfiltered and low-cut filtered set of representative shot gathers for each time step. The bandwidth of ground roll and guided wave amplitudes greater than noise recorded on unfiltered shot gathers was recorded. Likewise, the bandwidth of the first arrival, Haskell Limestone reflection, Stoner Limestone reflection, and air-coupled wave amplitudes greater than noise recorded on low-cut filtered shot gathers was recorded (Table 6).

To determine if the arrival times of seismic events (Figure 27), in addition to spectral characteristics, were affected by repeat shots in the source hole, arrival times of the first critical refraction, Haskell and Stoner Limestone reflections, and the air-coupled wave were recorded from receiver 1016 on the station 1073 shot gather (Table 7).

To evaluate source wavelet consistency, the wavelet had to be extracted from each time step to qualitatively analyze how the source wavelet was affected by repeat shots down the same source hole. The convolutional model of the seismic trace $x(t)$ is:

Table 6 – Bandwidth of recorded wavefield components. The low and high ends of the usable bandwidth of the ground roll and guided waves (a) were determined from unfiltered shot gathers. Usable bandwidth of the air-coupled wave ("air wave"), Stoner Limestone reflection, and first arrival (b) were determined from low-cut filtered shot gathers. Ambient noise threshold was approximately 20 dB for each time step; amplitudes of a wavefield component above this level were considered part of the usable bandwidth.

(a)

Time Step	Ground Roll Low	Ground Roll High	Guided Wave Low	Guided Wave High
1	0	245	0	340
2	0	250	0	340
3	0	250	0	340
4	0	255	0	340
5	0	255	0	340
6	0	255	0	340
7	0	245	0	340
8	0	245	0	350
9	0	250	0	350
10	0	240	0	345

(b)

Time Step	Air wave Low	Air wave High	Reflection Low	Reflection High	First Arrival Low	First Arrival High
1	45	370	100	370	0	410
2	60	380	70	400	0	420
3	25	360	70	400	0	430
4	45	360	75	415	0	430
5	45	360	80	420	0	440
6	30	365	70	410	0	440
7	40	380	80	400	0	440
8	45	340	80	420	0	435
9	50	360	80	410	0	440
10	50	360	80	410	0	440

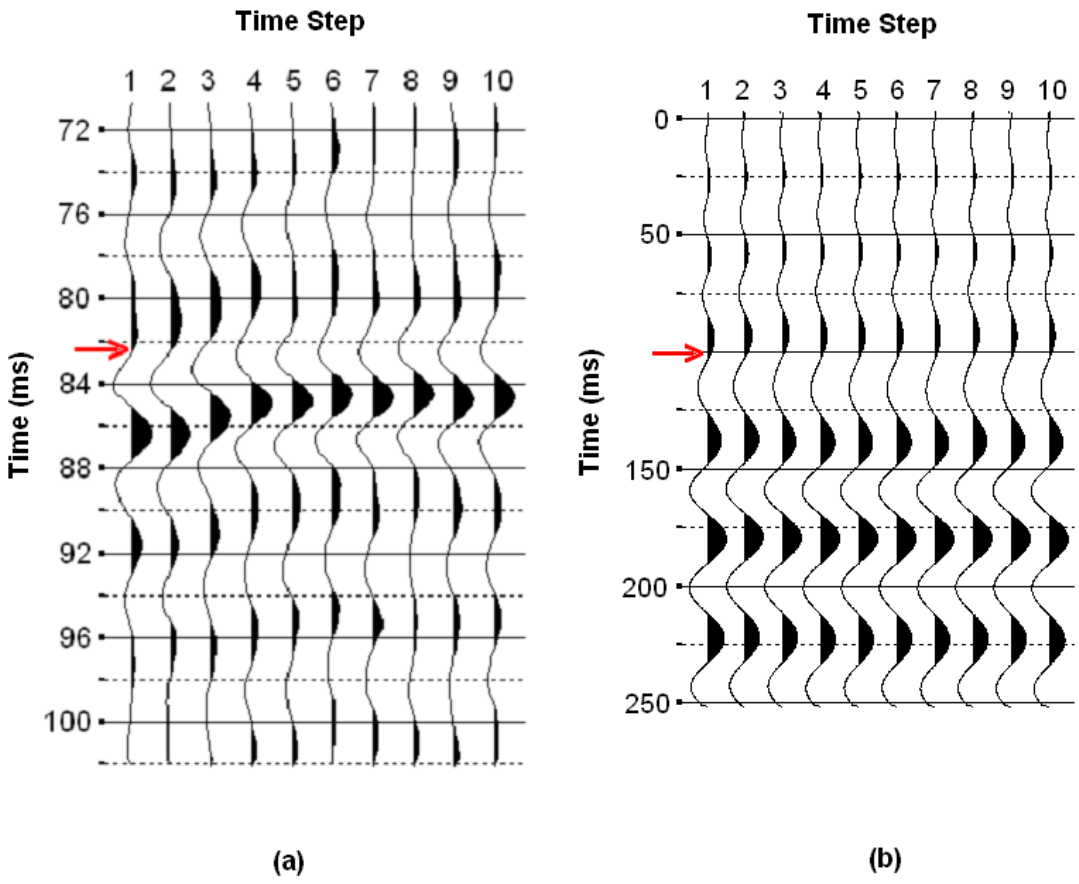

Figure 27 – Arrival of seismic events. The (a) Haskell Limestone reflection and (b) ground roll on the trace corresponding to source and receiver stations 1073 and 1016, respectively, in each time step. The arrival is marked with a red arrow for the first time step. Uncertainty in arrival time is plus or minus one sample (0.25 ms).

Table 7 - Arrival time of seismic events. Arrival time (a) and change in arrival time (b), in milliseconds, of the first arrival, Haskell and Stoner Limestone reflections, and air-coupled wave recorded by receiver 1016 when the source was at station 1073 for each time step. The first three events follow a similar pattern; the air-coupled wave changes very little.

(a)

Time Step	1	2	3	4	5	6	7	8	9	10
First Arrival	31.5	31.5	30.75	30.25	30	29.75	30	29.75	30	29.75
Haskell Limestone	42.75	43	42.25	41.5	41	40.75	41	40.75	41	41
Stoner Limestone	82.5	82.5	81.75	81	81.25	80.75	80.75	80.75	81	80.75
Air-Coupled Wave	106.75	106.75	106.75	107	107.25	107.25	107.25	107	107.25	107.25
Ground Roll	103	102.75	102.25	103	103	103	103	102.5	102.75	102.75

(b)

Time Step	1	2	3	4	5	6	7	8	9	10
First Arrival	0	0	-0.75	-1.25	-1.5	-1.75	-1.5	-1.75	-1.5	-1.75
Haskell Limestone	0	0.25	-0.5	-1.25	-1.75	-2	-1.75	-2	-1.75	-1.75
Stoner Limestone	0	0	-0.75	-1.5	-1.25	-1.75	-1.75	-1.75	-1.5	-1.75
Air-Coupled Wave	0	0	0	0.25	0.5	0.5	0.5	0.25	0.5	0.5
Ground Roll	0	-0.25	-0.75	0	0	0	0	-0.5	-0.25	-0.25

$$x(t) = w(t) * e(t)$$

where $w(t)$ is the source wavelet and $e(t)$ is the earth's impulse response (Yilmaz 2001). This model assumes that the earth consists of horizontal layers of constant velocity, the seismic source generates a compressional plane wave, the source wavelet is consistent throughout the subsurface, the seismic trace is noise-free, and the reflectivity series is random, which implies that it is infinite (Claerbout, 1976). If the assumptions of the convolutional model are true, most especially the infinite and random reflectivity assumption, the autocorrelation of the seismic trace can be used to determine the amplitude and phase spectra of the source wavelet (Claerbout, 1976, Robinson and Treitel, 1980; Yilmaz, 2001).

For conventional reflection seismology, the convolutional model assumptions are reasonably close to and assumed valid (Yilmaz, 2001). For near-surface seismology, in general, reflectivity is not infinite and random. Therefore, autocorrelation cannot be used to estimate the source wavelet. For time-lapse reflection seismology, it is not change in the source wavelet itself, but change in reflection wavelets that are of most concern. Therefore, spectral characteristics of reflection wavelets are examined instead of the estimated source wavelet.

To avoid altering the phase spectra of a wavelet, including some white noise arriving before and after is advisable when muting all other recorded energy on the trace. The Stoner Limestone reflection wavelet on the trace corresponding to source

and receiver stations 1073 and 1016 was selected for analysis because it was relatively free of coherent noise and contains 10 ms of approximately white noise before and after the reflection. All recorded energy except the reflection wavelet and noise surrounding it were muted on this trace from each time step and transformed into the frequency domain. Change in phase spectra (Figures 28 and 29) were analyzed for each.

A common technique to calculate time-lapse anomalies is to create amplitude difference sections by subtracting amplitudes on the CMP stacked section of the baseline survey from amplitudes on CMP stacked sections of subsequent monitor surveys (Greaves and Fulp, 1987; Lumley, 2004). To determine which time step (when used as the baseline) resulted in the minimal time-lapse anomaly, a CMP stacked section was created for each time step using the same processing flow. Field data were filtered with the 100-200 Hz low-cut filter and corrected for spherical divergence. All energy prior to and including the first arriving wavelets, and clipped data (due to the source overdriving the nearest receivers) were muted. Traces were gathered into CMPs, corrected for normal moveout, and CMP stacked. The average amplitude of the time-lapse signal was calculated for each difference section, first using the first time step as the baseline, then the second time step as the baseline, etc.

To approximate the time-lapse signal caused by ambient noise, all signal except ambient noise arriving before the first arrival was muted from low-cut filtered shot gathers. The processing procedure described above was repeated for these shot gathers containing only ambient noise (Table 8).

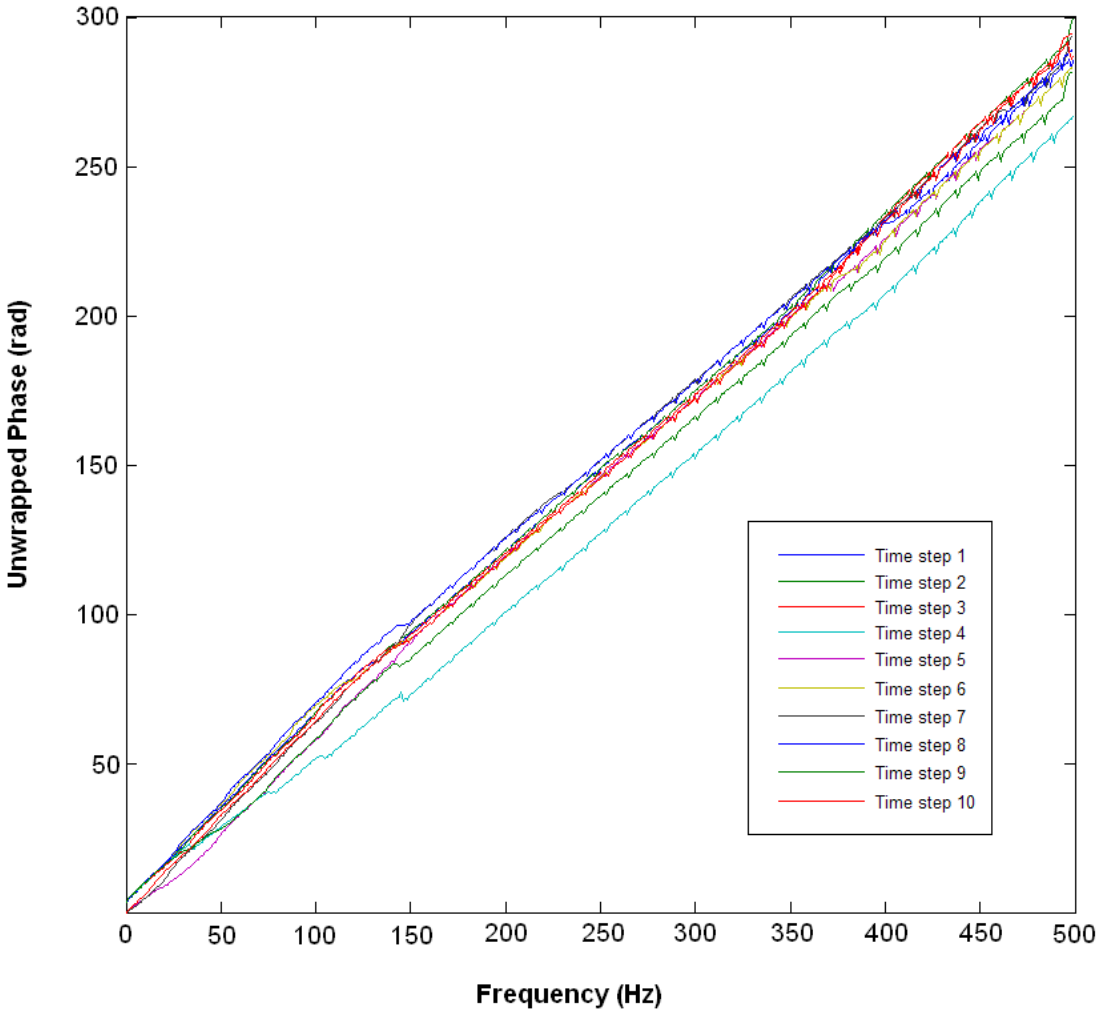

Figure 28 – Phase spectra of reflection wavelet. The (unwrapped) phase spectra were calculated for the Stoner Limestone reflection in each time step.

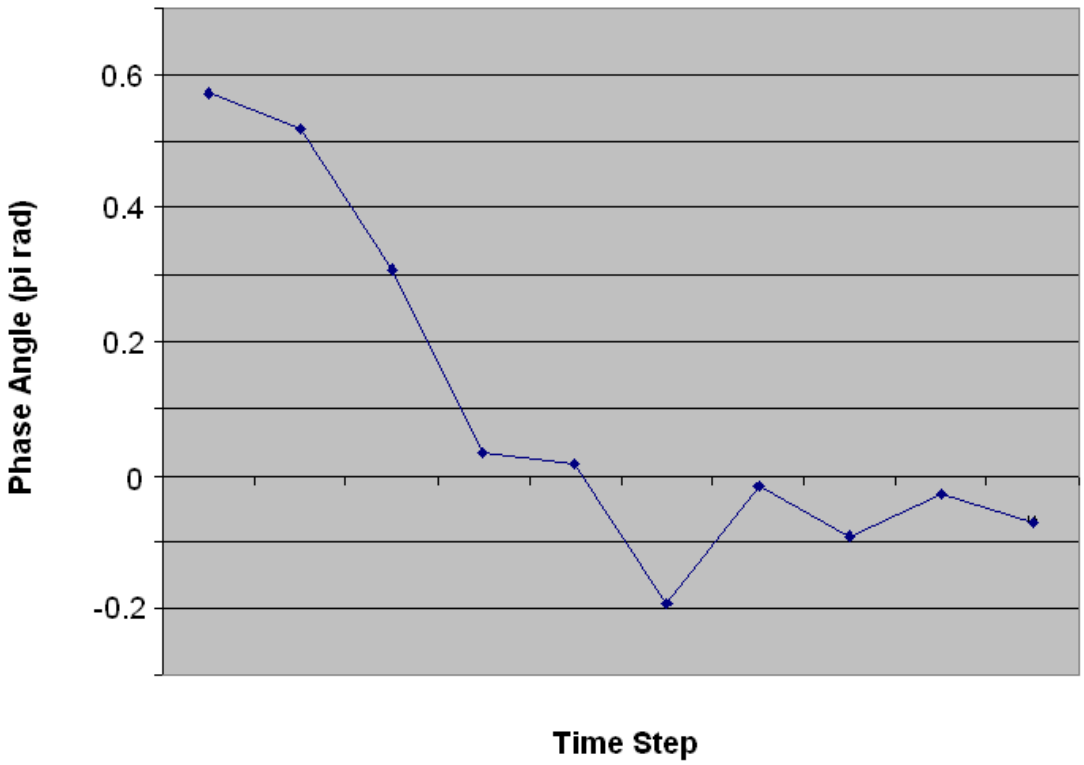

Figure 29 – Phase angle of the 200-Hz component. To determine the approximate pattern in which the phase spectra of the reflection wavelet in Figure 27 changed, the phase angle of the 200-Hz component is plotted for each time step.

Table 8 –Amplitudes of difference sections. Average amplitude before and after subtracting the average amplitude in the time-lapse signal caused by ambient noise using the first (a) and fourth (b) time steps as the baseline. The number of decibels greater than the resultant amplitude using the fourth time step as the baseline is listed.

	Time Step	Total Amplitude	Total Samples	Average Amplitude	Average minus noise	dB greater
	2	448441000	89336	5020	397910863	
	3	499060000	89336	5586	444452081	
(a)	4	516359000	89336	5780	460019421	
	5	501588000	89336	5615	446437613	9.3
	6	501933000	89336	5618	445994265	8.1
	7	499943000	89336	5596	442680071	8.5
	8	497868000	89336	5573	442350070	7.8
	9	489116000	89336	5475	432572736	7.8
	10	494473000	89336	5535	437838158	7.6
	5	172347000	89336	1929	153083044	
(b)	6	195739000	89336	2191	175657747	
	7	185981000	89336	2082	166519602	
	8	201296000	89336	2253	180727907	
	9	194322000	89336	2175	176809760	
	10	201306000	89336	2253	182453200	

Changes in the entire recorded wavefield resulting from firing multiple shots into the same source hole can be determined using the results of the aforementioned analyses. From these observations, recommendations can be made for optimizing the effectiveness of repeat firing for improving signal-to-noise ratio, resolution, and repeatability during time-lapse studies.

Discussion

Examining each component of the wavefield reveals that the total wavefield amplitude decreased significantly after the first time step (Table 5). During the second time step, the ground roll amplitude decreased by 54%, relative to the initial amplitude. As well, the guided wave amplitude decreased 47%, the first arrival amplitude decreased 46%, the Haskell Limestone reflection decreased 45%, the Stoner Limestone reflection amplitude decreased 56%, and the air-coupled wave amplitude decreased 56%.

Total source energy generated at the instant of detonation is approximately the same for each shot. Therefore, the apparent higher levels of seismic energy measured from the first downhole shot compared to subsequent shots must relate to source coupling. This decrease in source coupling appears to coincide with the observation that the gun recoil was much more evident for shots following the first shot at a station. Both of these observations support the suggestion that plastic deformation (i.e. compaction) of the hole wall material as a result from the first shot inhibited transmission of energy across the hole wall interface for later shots. This increased

wall compaction resulted in an increased rejection of the pressure wave and, thus, increased the observed gun recoil and decreased the total recorded wavefield amplitude. Suggestion that optimal source coupling for the first downhole shot is related to compaction agrees with the fact that transmission is favored across gradational interfaces (Kelly et al., 2002; Aki and Richards, 1980).

No significant change was observed in the dominant frequency of ground roll and guided waves (Table 5). Standard deviations over the ten time steps at any single station were generally less than 1 Hz. Likewise, the first arrival frequency band had a standard deviation of approximately 3 Hz. Reflection wavelet dominant frequencies changed significantly throughout the ten time steps. The average standard deviation in over the ten time steps is 13 Hz. In general, the dominant reflection wavelet frequency was lowest during the first time step, and increased during later time steps. Dominant frequency of both the first arrival, and Haskell Limestone and Stoner Limestone reflections increased non-linearly until it reached a maximum around the fifth time step, where it remained relatively consistent through the remaining records (Figure 30).

The change in useable bandwidth was ±15 Hz at most for ground roll and guided waves (Table 6). The bandwidth of higher frequency components of the wavefield changed more significantly. The bandwidth of the first arrival varied ±30 Hz throughout the time steps. Likewise, the Stoner Limestone reflection and the air-coupled wave varied ±70 and ±45 Hz, respectively. The useable bandwidths of body waves were relatively consistent in the third through the tenth time steps.

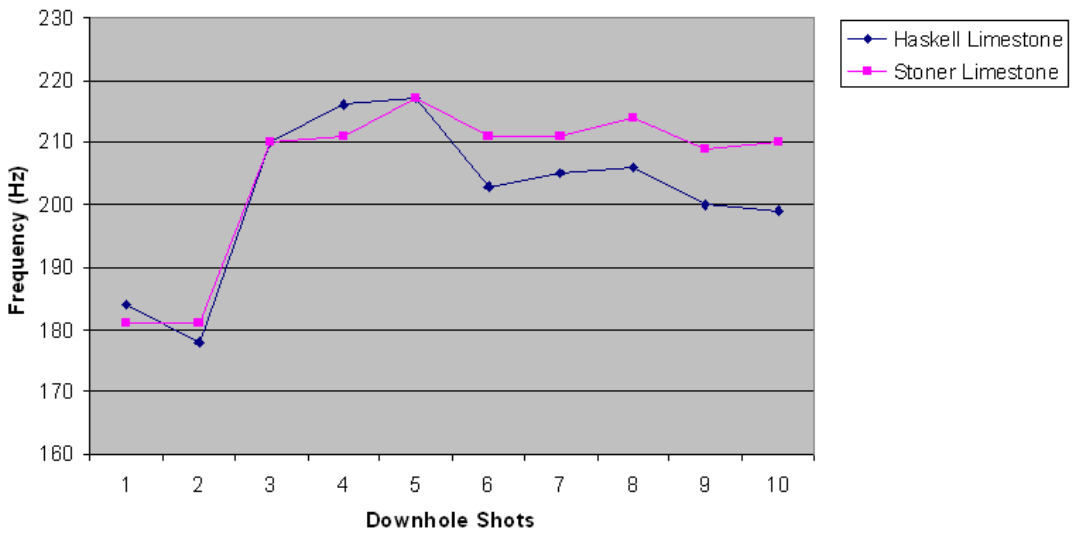

Figure 30 – Dominant reflection frequency. Dominant frequency of both the Haskell and Stoner Limestone reflections during each time step, calculated from shot records corresponding to source station 1067.

Arrival times of body waves changed very little in the second time step with respect to the first (Table 7). There was an increase during the third, and arrival time then stabilized in the fourth through tenth time steps. There was no significant (greater than plus or minus one time sample) change in arrival times of the air-coupled wave, indicating that the change in reflection arrival times is not caused by an inconsistent time break. There was no significant change in ground roll arrival times, indicating that the entire wavefield was not affected uniformly (i.e. compressional waves were affected differently than ground roll). Therefore, a static time shift could not be applied to correct the different reflection arrival times.

Phase angle of the 200-Hz component of the Stoner Limestone reflection wavelet changes very little in the second time step (with respect to the first). The third and fourth downhole shots, however, resulted in increasingly negative phase angles. Phase angle stabilizes and is relatively consistent for the fourth through tenth time steps (Figure 29).

Changes in dominant frequency and usable bandwidth were observed for the entire recorded wavefield, and changes in the phase spectra were observed for the Stoner Limestone reflection wavelets. These observations suggest that plastic deformation affects the process of energy transmission across the hole wall interface. In general, spectral characteristics and arrival times of body waves were more sensitive to plastic deformation of the hole wall sediment than those of ground roll. The implication is that firing multiple shots to condition pre-drilled holes could separate these two components of the wavefield. Separation is advantageous because

ground roll tends to mask desired reflection signals (Sheriff, 2002) and is generally difficult to remove (Karsli and Bayrak, 2004).

When the inelastic processes minimized after the fourth downhole shot, the recorded wavefield is more consistent through the tenth time step. When the fourth time step is used as the baseline survey, the amplitude of the time-lapse signal is approximately 8 dB less than when the first time step is used as the baseline, even when the effect of ambient noise is subtracted. Therefore, using the first time step as the baseline contributes to significantly greater error in the time-lapse signal than using the fourth time step as the baseline. Three downhole shots should be fired to properly condition dry pre-drilled source holes in this setting.

Conclusions

The first downhole shot results in the greatest recorded wavefield amplitudes in this particular geologic setting, suggestive of the best source coupling. Total recorded wavefield amplitude is consistent from the second through the tenth time steps. Repeatedly firing the source into the same source hole caused plastic deformation of the hole wall sediment, which affected the transmission of energy across the interface. Body waves are more sensitive to this plastic deformation than ground roll. Average spectral characteristics (dominant frequency, usable bandwidth, and phase response) of the reflection wavelets appear most consistent from the fourth through the tenth time steps. Because data characteristics are most consistent after the fourth time step, three shots should be fired downhole at this site to properly

condition holes prior to acquisition of reflection events for repeatability studies. The fourth downhole shot should be used as the baseline.

Characteristics of data from near-surface time-lapse surveys vary throughout the time steps, and ideal processing parameters for the baseline may not be ideal for later time steps. Optimal processing parameters are designed based on characteristics of data from all time steps. Only zero-phase-response digital frequency filters are recommended. If phase-lag filters are used, they must be used with caution, and only when phase spectrum of the source wavelet is extremely consistent throughout the time-lapse survey. As recommended by Porter-Hirsche and Hirsch (1998) the use of statistical processing techniques should be avoided to prevent, for example, inducing time-lapse noise resulting from different phase responses in different time steps.

Prior to a near-surface time-lapse seismic survey, it would be advantageous to fire multiple shots in a test hole at the planned survey site. These data could be used to determine acquisition parameters that would optimize consistency and minimize time-lapse anomalies not associated with subsurface change.

Final Conclusions

Repeatability of Vibroseis data is affected by source and receiver terrains. This study found that source station terrains that optimize repeatability are those with perennial vegetation and no or minimal human traffic, such as vegetated sand dunes or sod-covered livestock pastures. Source station terrains that result in poor repeatability are those that are affected by human traffic, such as roads and tilled

fields. Other studies have found that rigid surfaces cause decoupling of the baseplate with the ground surface, resulting in harmonic distortion of the vibrator signal (Schrodt, 1987; Reust, 1995). Harmonic distortion of the signal may not be repeatable at a site and, therefore, source station terrains that reduce harmonic distortion optimize repeatability. In my study, this is demonstrated by roads resulting in poor repeatability and sand dunes resulting in comparatively good repeatability.

Data characteristics from multiple shots recorded at hole wall sediment deform plastically at a non-linear, complex rate through at least the first ten shots. Deformation alters energy is transmission across the hole/sediment interface, as evidenced by changes in amplitude and phase spectra, and arrival times of recorded seismic events. Compressional waves and ground roll responded differently to deformation. This observation has potential application to wavefield separation. Prior to any planned time-lapse survey, it would be advantageous to fire multiple shots in a test hole to monitor changes in the wavefield. Determining how many shots should be fired to properly condition the hole is essential for optimized repeatability of the desired wavefield components.

References

Aki, K., and P.G. Richards, 1980, Quantitative Seismology: Theory and Methods: W.H. Freeman and Company.

Anderson, K.L., 1953, Utilization of Grasslands in the Flint Hills of Kansas: Journal of Range Management, **6**, 86-93.

Arbogast, A.F., and W.C. Johnson, 1996, Surficial Geology and Stratigraphy of Russell County, Kansas: Kansas Geological Survey.

Aritman, B.C., 2001, Repeatability study of seismic source signatures: Geophysics, **66**, 1811-1817.

Baker, G.S., D.W. Steeples, C. Schmeissner, and K.T. Spikes, 2000, Ultrashallow seismic reflection monitoring of seasonal fluctuations in the water table: Environmental and Engineering Geoscience, **6**, 271-277.

Birkelo, B.A., D.W. Steeples, R.D. Miller, and M. Sophocleous, 1987, Seismic reflection study of a shallow aquifer during a pumping test: Ground Water, **25**, 703-709.

Beaubouef, T., M. Wagaman, R. Sfara, M. FitzMaurice, and B. Barrett, 2005, Use of airborne LiDAR in the full cycle of onshore hydrocarbon exploration: a legacy dataset: 75th Annual International Meeting, SEG, Expanded Abstracts, 60-63.

Brittle, K.F., L.R. Lines, and A.K. Dey, 2001, Vibroseis deconvolution: a comparison of cross-correlation and frequency-domain sweep deconvolution: Geophysical Prospecting, **49**, 675-686.

Calvert, R., 2005, 4D Technology: where are we, and where are we going?: Geophysical Prospecting, **53**, 161-171.

Claerbout, J.F., 1976, Fundamentals of Geophysical Data Processing: McGraw-Hill.

Crawford, J.M., W.E. Doty, and M.R. Lee, 1960, Continuous signal seismograph: Geophysics, **25**, 95-105.

Cox, M.J.G., 1999, Static Corrections for Seismic Reflection Surveys: Society of Exploration Geophysicists.

de Waal, H., and R. Calvert, 2003, Overview of global 4D seismic implementation strategy: Petroleum Geoscience, **9**, 1-6.

Dickey, H.P., J.L. Zimmerman, R.O. Plinsky, and R.D. Davis, 1977, Soil Survey of Douglas County, Kansas: United States Department of Agriculture Soil Conservation Service, 73 p.

Ebrom, D., P. Krail, D. Ridyard, and L. Scott, 1998, 4-C/4-D at Teal South: The Leading Edge, **17**, 1450-1453.

Esquivel, M., 2005, Geotechnical Engineering Study: Rio Grande Levee & US 28, Las Cruces, New Mexico: Eng. Study Report to Joseph Dunbar USACE Vicksburg, MS, 15 p.

Gibson, B., and K. Larner, 1984, Predictive deconvolution and the zero-phase source: Geophysics, **49**, 379-397.

Greaves, R.J., and T.J. Fulp, 1987, Three-dimensional seismic monitoring of an enhanced oil recovery process: Geophysics, **52**, 1175-1187.

He, W., R.N. Anderson, L. Xu, A. Boulanger, B. Meadow, and R. Neal, 1996, 4D seismic monitoring grows as production tool: Oil and Gas Journal, **94**, 41-46.

Hoover, G.M., and J.T. O'Brien, 1980, The influence of the planted geophone on seismic land data: Geophysics, **45**, 1239-1253.

Huang, X., L. Meister, and R. Workman, 1998, Improving production history matching using time-lapse seismic data: The Leading Edge, **12**, 1430-1433.

Janson, E., 2001, Improving the repeatability for 4D time lapse seismic: First Break, **19**, 32-37.

Jantz, D.R., W.A. Wehmueller, and H.D. Owens, 1982, Soil Survey of Russell County, Kansas: United States Department of Agriculture Soil Conservation Service, 103 p.

Jefferson, R.D., D.W. Steeples, R.A. Black, and T. Carr, 1998, Effects of soil-moisture content on shallow-seismic data: Geophysics, **63**, 1357-1362.

Karsli, H., and Y. Bayrak, 2004, Using the Wiener-Levinson algorithm to suppress ground roll: Journal of Applied Geophysics, **55**, 187-197.

Keller, G.R., and S.M. Cather, 1994, Basins of the Rio Grande rift: Structure, stratigraphy, and tectonic setting: Geological Society of America Special Paper 291, 304 pp.

Kelly, M.C., C. Skidmore, and D. Ford, 2002, Prediction of bed geometry, net and gross reservoir thickness: 72nd Annual International Meeting, SEG, Expanded Abstracts, 1782-1784.

Knapp, R.W., 1988, High resolution seismic data of Pennsylvanian cyclothems in Kansas: The Leading Edge, **17**, 24-27.

Lambrecht, J.L., and R.D. Miller, 2006, Catastrophic sinkhole formation in Kansas: A case study: The Leading Edge, **25**, 342-347.

Li, G., G. Purdue, S. Weber, and R. Couzen, 2001, Effective processing of nonrepeatable 4-D seismic data to monitor heavy oil SAGD steam flood, East Senlac, Saskatchewan, Canada: The Leading Edge, **20**, 54-63.

Lillie, R.J., 1999, Whole Earth Geophysics: An Introductory Textbook for Geologists and Geophysicists: Prentice Hall.

Lumley, D.E., 2004, Business and technology challenges for 4D seismic reservoir monitoring: The Leading Edge, **23**, 1166-1168.

Mack, G.H., 1997, The Geology of Southern New Mexico: University of New Mexico Press.

McKenna, J., D. Sherlock, and B. Evans, 2001, Time-lapse 3-D seismic imaging of shallow subsurface contaminant flow: Journal of Contaminant Hydrology, **53**, 133-150.

Miller, R.D., R.D. Markiewicz, T.R. Rademacker, R. Hopkins, R.J. Rawcliffe, and J. Paquin, 2007, Advantages of wet work for near-surface seismic reflection: 77th Annual International Meeting, SEG, Expanded Abstracts, 1147-1151.

Miller, R.D., S.E. Pullan, D.W. Steeples, and J.A. Hunter, 1992, Field comparison of shallow seismic sources near Chino, California: Geophysics, **57**, 693-709.

Miller, R.D., S.E. Pullan, D.W. Steeples, and J.A. Hunter, 1994, Field comparison of shallow P-wave seismic sources near Houston, Texas: Geophysics, **59**, 1713-1728.

Miller, R.D., S.E. Pullan, J.S. Waldner, and F.P. Haeni, 1986, Field comparison of shallow seismic sources: Geophysics, **51**, 2067-2092.

Moussa, R., M. Voltz, and P. Andrieux, 2002, Effects of the spatial organization of agricultural management on the hydraulic behaviour of a farmed catchment during flood events: Hydrological Processes, **16**, 393-412.

O'Conner, H.G., 1960, Geology and Ground-water Resources of Douglas County, Kansas: Kansas Geological Survey, Bulletin 148, 200 p.

Porter-Hirsche, J., and K. Hirsche, 1998, Repeatability Study of Land Data Acquisition and Processing for Time Lapse Seismic: 68th Annual International Meeting, SEG, Expanded Abstracts, 9-11.

Qian, R., Y. Hu, P. Li, L. Xu, and Y. Xiang, 2006, Challenges and solutions for land seismic exploration in China: The Leading Edge, **25**, 1380-1382.

Rademacker, T.R., 2006, Optimizing High-frequency Vibroseis Data: Kansas Geological Survey, Open-file report 2006-32, 86 p.

Raef, A.E., R.D. Miller, A.P. Byrnes, and W.E. Harrison, 2004, 4D seismic monitoring of the miscible CO2 flood of Hall-Gurney Field, Kansas, U.S.: The Leading Edge, **23**, 1171-1176.

Raef, A.E., R.D. Miller, E.K. Franseen, A.P. Byrnes, W.L. Watney, and W.E. Harrison, 2005, 4D seismic to image a thin carbonate reservoir during a

miscible CO_2 flood: Hall-Gurney Field, Kansas, USA: The Leading Edge, **24**, 521-526.

Reust, D.K., 1995, Vibrator force control: How simple can it get?: The Leading Edge, **14**, 1129-1133.

Rickett, J., and D. Lumley, 2001, Cross-equalization data processing for time-lapse seismic reservoir monitoring: A case study from the Gulf of Mexico: Geophysics, **66**, 1015-1025.

Robertsson, J.O.A., A. Pugin, K. Holliger, and A.G. Green, 1995, Effects of near-surface waveguides on shallow seismic data: 65th Annual International Meeting, SEG, Expanded Abstracts 1329-1332.

Robinson, E.A., and S. Treitel, 1980, Geophysical Signal Analysis: Prentice-Hall, Inc.

Ross, C.P., and M.S. Atlan, 1997, Time-lapse seismic monitoring: Some shortcomings in nonuniform processing: The Leading Edge, **16**, 1021-1027.

Ross, C.P., G.B. Cunningham, and D.P. Weber, 1996, Inside the crossequalization black box: The Leading Edge, **15**, 1233-1240.

Sallas, J.J., 1941, Seismic vibrator control and the downgoing P-wave: Geophysics, **49**, 732-740.

Sheriff, R.E., 2002, Encyclopedic Dictionary of Applied Geophysics: Society of Exploration Geophysicists.

Schrodt, J.K., 1987, Techniques for improving Vibroseis data: Geophysics, **52**, 469-482.

Schulmeister, M.K., J.J. Butler Jr., J.M. Healey, L. Zheng, D.A. Wysocki, and G.W. McCall, 2003, Direct-Push Electrical Conductivity Logging for High-Resolution Hydrostratigraphic Characterization: Ground Water Monitoring and Remediation, **23**, 52-62.

Sloan, S.D., G.P. Tsoflias, and D.W. Steeples, 2007, Seismic AVO variations related to partial water saturation during a pumping test: 77th Annual International Meeting, SEG, Expanded Abstracts, 1212-1216.

Steeples, D.W., R.D. Miller, and R.W. Knapp, 1987, Downhole .50-caliber rifle: An advance in high-resolution seismic sources: 57th Annual International Meeting, SEG, Expanded Abstracts, 76-78.

Taylor, J.R., 1997, Error Analysis: the study of uncertainties in physical measurements: University of Science Books.

Vesnaver, A.L., F. Accaino, G. Bohm, G. Mandrussani, J. Pajchel, G. Rossi, and G. Dal Moro, 2003, Time-lapse tomography: Geophysics, **68**, 815-823.

Watney, W.L., 1980, Cyclic sedimentation of the Lansing and Kansas City Groups (Missourian) in northwestern Kansas and southwestern Nebraska: A guide for petroleum exploration: Kansas Geological Survey, Bulletin 220, 72 p.

Watney, W.L., 1985, Origin of four Upper Pennsylvanian (Missourian) cyclothems in the subsurface of western Kansas; application to search for accumulation of petroleum: Kansas Geological Survey, Open-file report 85-2, 524 p.

Yilmaz, O., 2001, Seismic Data Analysis: Processing, Inversion, and Interpretation of Seismic Data: Society of Exploration Geophysicists.

Zamorouev, A., D. Whitcombe, M. Dyce, and L. Hodgson, 2006, A simple methodology for 4D noise reduction and repeatability improvement: 76th Annual International Meeting, SEG, Expanded Abstracts, 3155-3159.